Isolated Bi-Directional DC-DC Converter with Smooth Start-up Transition

Shiwei Mao

Thesis submitted to the faculty of the
Virginia Polytechnic Institute and State University
in partial fulfillment of the requirements for the degree of

Master of Science
In
Electrical Engineering

Jih-Sheng Lai, Chair
Kathleen Meehan
Qiang Li

May 1st, 2015
Blacksburg, VA

Keywords: bi-directional, dc/dc, isolated, start-up, full-bridge, active clamp

Isolated Bi-Directional DC-DC Converter with Smooth Start-up Transition

Shiwei Mao

ABSTRACT

The bi-directional dc/dc converter is a very popular and effective tool for alternative energy applications. One way it can be utilized is to charge and discharge batteries used in residential solar energy systems. In the day, excess power from the PV panels is used to charge the batteries. During the night, the charged batteries will power the dc bus for loads in the house such as home appliances. The dual active bridge (DAB) converter is very useful because of its high power capability and efficiency. Its symmetry is effective in transferring power in both directions. However, the DAB converter has drawbacks in the start-up stage. These drawbacks in boost mode include high in-rush current during start-up, and the fact that the high side voltage cannot be lower than the low side voltage. A popular existing method to alleviate this problem is the use of an active clamp and a flyback transformer in the circuit topology to charge the high side before the converter is switched into normal boost operation. The active clamp not only helps eliminate the transient spike caused by the transformer leakage, but also continues to be used during steady state. However, this method introduces a new current spike occurring when the converter transitions from start-up mode to boost mode. To alleviate this new setback, an additional transitional stage is proposed to significantly reduce the current spike without the use of any additional components. The converter is current-fed on the low side, and voltage-fed on the high side. A simple phase shif

control is used in buck mode and PWM control is used during the boost mode for both the start-up mode and the normal boost operation. This thesis discusses the performance results of a 48-400 V dc/dc converter with 1000 W power output.

Acknowledgements

First, I would like to give my deepest and most sincere gratitude to my adviser Dr. Lai for challenging me and guiding me through my research. When I first started I had almost no experience in power electronics, his patience and guidance have taught me skills that will help me face problems for the rest of my life.

Secondly, I would like to express my appreciation to my committee members Dr. Meehan and Dr. Li. Dr. Meehan helped guide me through multiple undergraduate courses that helped me develop engineering skills that helped me through graduate school. Dr. Li's graduate course in power electronics helped me see the subject in a whole new way in which is both challenging and exciting.

Next, I would like to thank everyone in the FEEC lab. The knowledge the students in this lab possess is very inspiring. Much of my research would not have been possible without the help and support with my fellow lab mates. My special thanks go to Dr. Wensong Yu, Mr. Rui Chen, Mr. Zaka Zahid, Mr. Lanhua Zhang, Dr. Ruixiang Hao, Mr. Gary Kerr, Mr. Baifeng Chen, Mrs. Hongmei Wang, Mr. Nathan Kees, Mr. Bin Gu, Mr. Thomas LaBella, Mr. Seung-Ryul Moon, Mr. Hidekazu Miwa, Mr. Andy Poush, Mr. Cong Zheng, Mr. Eric Faraci, Mr. Bo Zhou, Mr. Weihan Lai, Mr. Jason Dominic, and Mr. Andrew Amrhein for helping me through the many challenges I have faced. Their support made a huge difference throughout my research.

Finally, I would like to express my gratitude to my parents for their encouragements throughout my whole life. Without them I would not be anywhere near where I am today. Next, my brother Jason Mao, girlfriend Lindsay Nevins, and friends Kevin Sprenger and Chris Jennette all helped me through the most stressful moments of

my life and encouraged me to keep going when I'm ready to give up. It is tough to find good friends like them and I will always be thankful for their help in getting me through the toughest challenge of my life so far.

All photos by author, 2015.

TABLE OF CONTENTS

TABLE OF FIGURES

CHAPTER 1: Introduction

1.1 Background

Isolated bi-directional dc/dc converters are widely used for standard applications such as battery chargers/dischargers, uninterruptible power supplies (UPSs), hybrid electric vehicle systems (HEVs), and alternative energy systems. These converters can produce eco-friendly energy, which is used by the applications above on a daily basis.

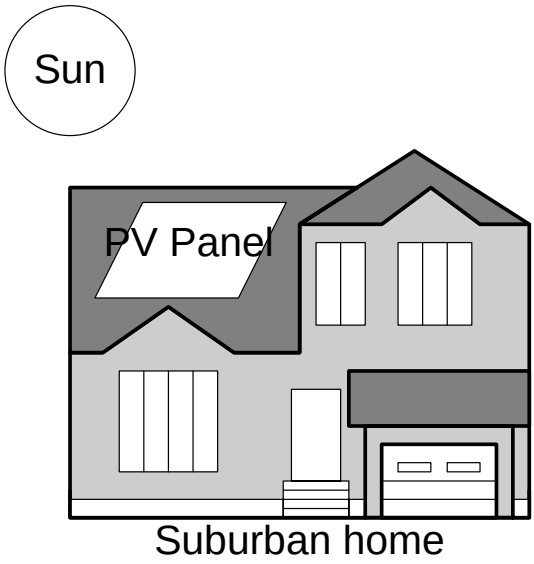

Fig. 1.1: Solar energy powered house

The primary application for the isolated bi-directional dc/dc converter is the charging/discharging of batteries. Figure 1.1 shows a house with attached solar panels used for some exemplary standard loads, such as home appliances, which can be powered by the bi-directional converter. In the application illustrated in Figure 1.1, energy

absorbed by photovoltaic (PV) panels is fed into a battery by the converter during the day with sufficient sunlight; at night, or when there is not enough sunlight, the battery discharges to supply power to a bus. Figure 1.2 shows the overall system of this bi-directional dc/dc converter. During the battery charging period, the bi-directional converter operates in buck mode. In some cases, the additional power from the PV panels may be provided to the loads in the house through the use of a dc/ac inverter. During the battery discharging period, the bi-directional converter operates in boost mode. The stored energy in the batteries is first used to power the 400 V dc bus, and is then fed into the same inverter to be used by the loads [1 - 3].

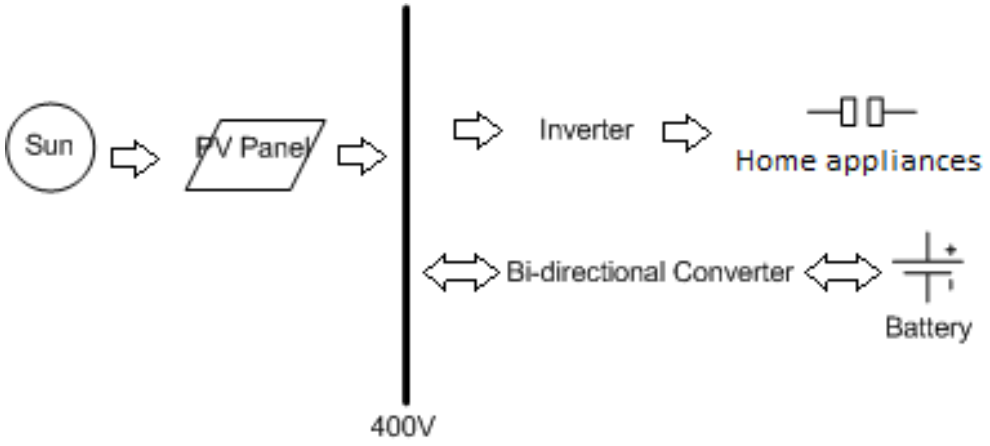

Fig. 1.2: System of this bi-directional dc/dc converter

1.2 Battery Charging Characteristics

The design and implementation of the charging phase of the system requires an understanding of the technical process of charging a battery. Batteries are devices composed of electrochemical cells capable of storing chemical energy, which is then converted into electrical energy. High performance batteries are typically able to hold a

charge for an extended time, operate safely under high power conditions, and complete charging and discharging cycles several times over the life of the battery. During most of a typical charging cycle, batteries charge in constant current (CC) mode. During this period the current flowing into the battery is constant and the voltage of the battery slowly rises. In addition, the current sensing must be very accurate to properly charge the battery, and the voltage level must be monitored. After a certain voltage level (different depending on the battery) has been reached, the battery charger switches to constant voltage (CV) mode. During CV charging, the voltage of the battery is kept constant and the current slowly decreases as the charge of the battery reaches a maximum capacity. Furthermore, the voltage sensing needs to be accurate and efficient, thereby maintaining the present charge while preventing overcharging the battery. Figure 1.3 shows the typical charging profile of a lithium ion (Li-ion) battery [4].

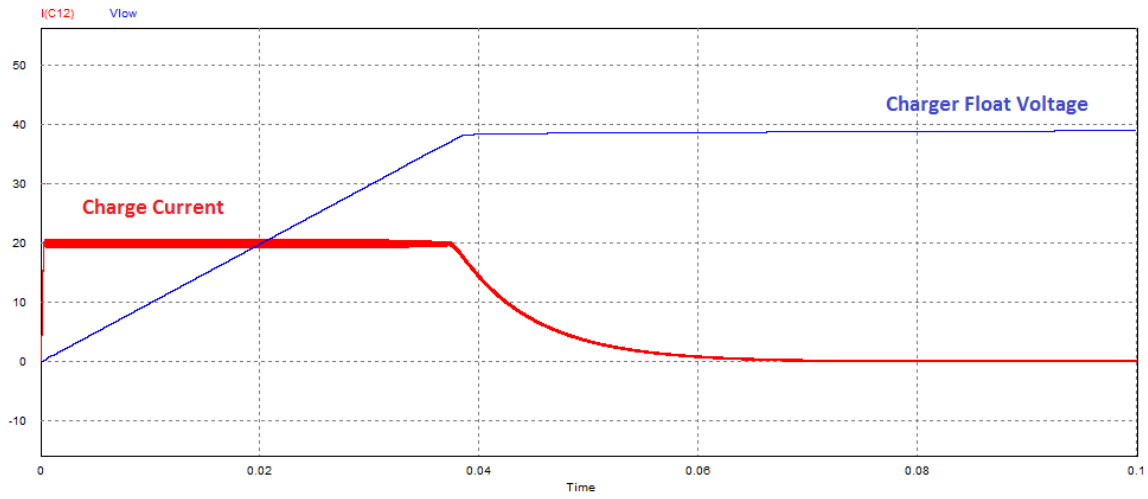

Fig. 1.3: Battery charging profile of Li-ion cell

As shown in Figure 1.3, the charge current (in blue) is initially steady in the constant current mode. The charger float voltage (in red) increases until a certain point is reached.

After this point, the charger switches to constant voltage mode where the charger float voltage is kept steady, and the charge current slowly drops as the charge capacity increases. During both CC and CV stages, the charge capacity is increasing. Upon the charge capacity reaching 100%, the charge current drops to zero. The charger is still operating in constant voltage mode, but the battery is no longer being charged.

In the application of this bi-directional dc/dc converter, the battery can be discharged completely then recharged to maximum capacity on a daily basis. The most effective way to do this is to have a system, which provides fast and efficient charging/discharging characteristics. The isolated bi-directional dc/dc converter is the battery charger/discharger of many solar energy systems and must accomplish the battery charging/discharging characteristics described [4].

1.3 Review and Selection of Switching Devices

In terms of switching devices, many options are available for power electronics applications. The most commonly used switching devices are metal-oxide semiconductor field-effect transistors (MOSFETs) and insulated-gate bipolar transistors (IGBTs). The selection of the switching devices is important for the most efficient switching.

Figures 1.4 and 1.5 show the symbols of a n-channel MOSFET and IGBT with anti-parallel diodes respectively. Both the MOSFET and the IGBT are voltage controlled devices.

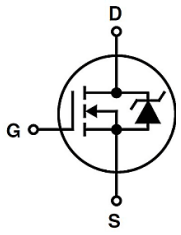

Fig. 1.4: Symbol of MOSFET with anti-parallel diode

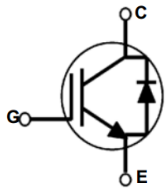

Fig. 1.5: Symbol of IGBT with anti-parallel diode

In typical applications, the MOSFETs are better suited for high frequency and low voltage scenarios. Contrarily, IGBTs are preferred in lower frequency and high voltage applications due to a tail current that exists during the transition from on to off. The presence of the tail current also makes IGBT's more favorable for lower duty cycle operations to avoid switching losses during turn-on [5].

In the case of this isolated bi-directional dc/dc converter, the primary side is low voltage while the secondary side is high voltage. Because of this, it is best to use MOSFETs on the primary side and IGBTs on the secondary side for switching applications.

1.4 Topology Review and Selection

The selection of the converter topology is one of the most critical aspects of converter design. For this thesis, the low voltage is 48 V and the high voltage is 400 V; because of this large difference in voltages, isolation is necessary for power conversion.

The isolated bi-directional dc/dc converter can be realized with several topologies, the most popular of which are the half-bridge and the full-bridge topologies [31]. Compared to the full-bridge topology, the half-bridge topology has the benefit of having fewer components, thus minimizing production costs. Having fewer switching components also reduces switching loss and simplifies gating controls (depending on operation and control theory). However, the full-bridge topology is more suitable for high power applications, despite the increased size and cost. For the purpose of this thesis, the full-bridge converter appears to be more appropriate, but both topologies will be discussed thoroughly.

1.4.1 Half-bridge Topology Review

The half-bridge topology is capable of handling lower power conversion (under 500 watts). This converter topology is appealing due to its low cost, small size, and simplicity.

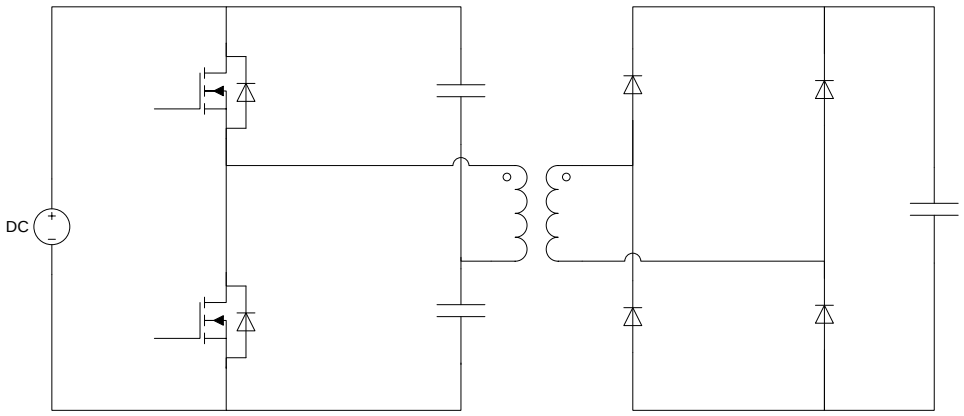

Fig. 1.6: Schematics of the half-bridge topology

Figure 1.6 shows a standard half-bridge topology of a uni-directional dc/dc converter. In order to change the uni-directional topology to bi-directional, the diodes from the rectifier side must be replaced with active components.

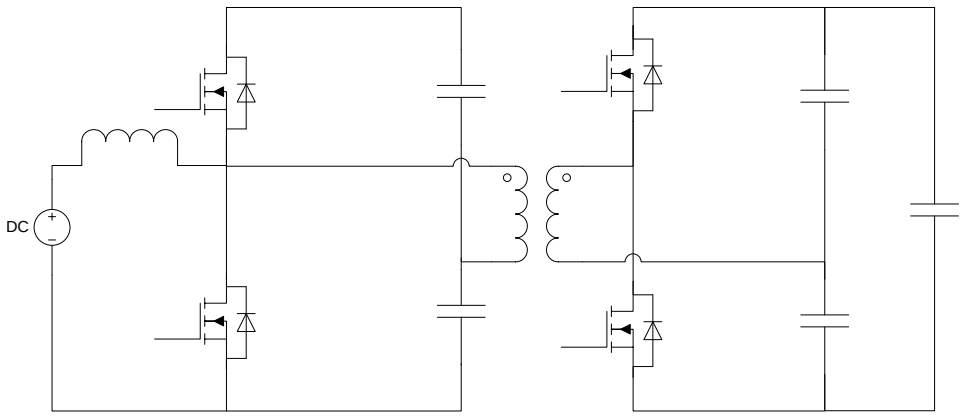

Fig. 1.7: Half-bridge bi-directional dc/dc converter topology

Figure 1.7 shows the standard half-bridge topology of the bi-directional dc/dc converter. As illustrated, the diodes on the secondary side of the transformer are replaced to reflect the primary side for bi-directional operation. This topology uses a total of four active switching components, and includes a current fed primary side and a voltage-fed secondary side [6 - 8].

The topology in Figure 1.7 can be used as a base circuit for many different applications. H. Fan and H. Li [9] combined multiple half-bridge converters in a cascaded manner to handle higher voltage levels (above 500 watts). This results in the use of lower voltage handling MOSFET's and a high power low volume solid state transformer operating in higher frequencies. Although the converter can efficiently handle high voltage, the cost of many more components, as well as the complexity in driving all the switching devices simultaneously make the topology of H. Fan and H. Li [9] inappropriate for the thesis. Another application uses an additional bridge to provide

the bi-directional converter with additional ports. L. Wang, Z. Wang, and H. Li [10] study the bi-directional converter with three ports. Having more ports can potentially make the system more stable in terms of each port having more options for useable power, but it is also more costly and difficult for control. Choi, Ju, Park, Kim, and Lim [11] disclose an uninterruptible power source (UPS) system with a half-bridge bi-directional dc/dc converter, wherein the UPS is used as a back-up power supply instead of the primary power supply. As a result, the battery would not be charged and discharged on a daily basis and would consequently prolong the life of the battery. However, the use of the battery to power the house loads at night is much cheaper in terms of electricity costs. In another study done by Yang and Liang [12], the transformer in the converter is removed but the converter still functions in bi-directional manner. As a result, the overall size and cost of the converter is reduced. However, this converter is limited in the ability to provide different voltage levels. The isolation requirement is also not met by Yang and Liang's study.

1.4.2 Full-bridge Topology Review

The full-bridge topology is more appealing than the half-bridge when it comes to high power applications. Having twice as many switching components also means that the full-bridge topology can handle twice as much power as the half-bridge topology. The symmetry of the full bridge dc/dc converter makes this topology a very good choice with balanced results for both directions of power conversion. Ideally speaking, because most switching devices such as MOSFETs and IGBTs have intrinsic anti-parallel body

diodes, an H bridge of these switches in the off state is a rectifier. The gating signals can be controlled to determine the direction of power flow [13].

However, the full-bridge topology has several drawbacks, among which the most severe is the high in-rush current during the start-up of the boost mode because the high side voltage is low. In addition, there is a transient voltage spike due to the leakage inductance of the transformer [14]. Therefore, to use the full-bridge topology, these problems must be eliminated.

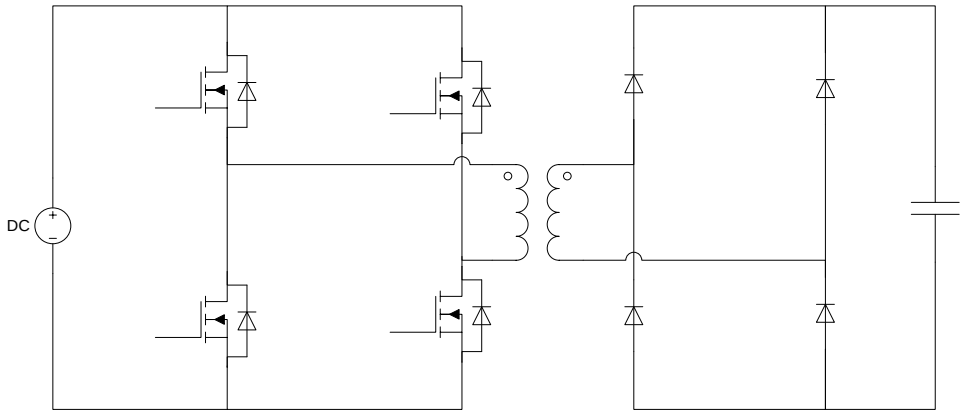

Fig. 1.8: Schematics of the uni-directional full-bridge topology

Although similar to the half-bridge topology shown in Figure 1.6, the full-bridge topology shown in Figure 1.8 has twice as many transistors as the half-bridge topology [15]. In order to change the uni-directional topologies to bi-directional, the diodes from the rectifier side must be replaced with active switches.

The implementation of the isolated bi-directional dc/dc converter can be done in several additional different ways. The topology of T. Hirose and H. Matsuo [16-18] in their study on the bi-directional converter is attractive in terms of the high efficiency and the active bridges being “superposed”. The superposed topology of the high voltage side

and the low voltage side means that the high side voltage is always at least the same voltage as the low side voltage, eliminating the start-up problem. However, while this superposed strategy solves the start-up problem which is the main vulnerability of the full-bridge, the superposed converter does not provide the proper isolation that is required to prevent problems, such as electric shock and noise, caused by the large difference in voltage levels between the high and low voltage sides.

F. Krismer, J. Biela, and J.W. Kolar [19, 20] disclose several evaluations of isolated bi-directional dc/dc converters with the full-bridge topology. Figure 1.9 shows the topologies that were analyzed. Figure 1.9(a) is the standard full-bridge topology, and is the fundamental circuit for the additional topologies. Figures 1.9(b) incorporates a resonant block in between the high side and the low side in the form of a capacitor. Figure 1.9(c) incorporates a voltage regulator is located near the high side bus to help the performance of the converter under wide output voltage range. Figure 1.9(d) incorporates both additional circuits for increased performance and functionality.

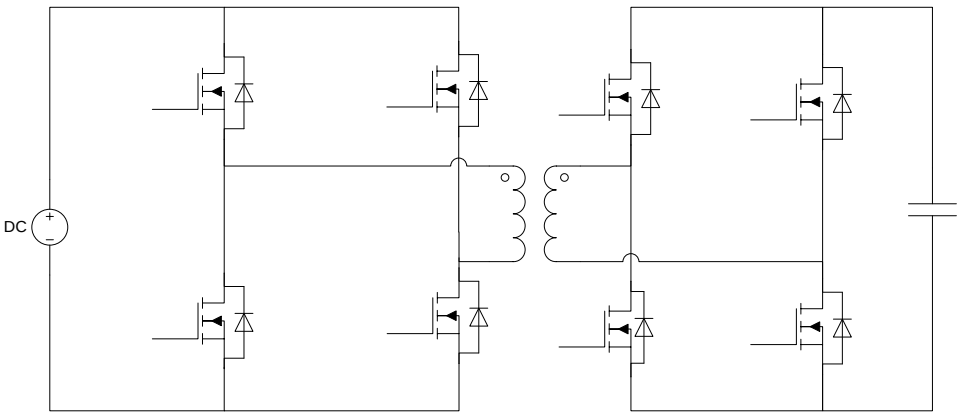

(a)

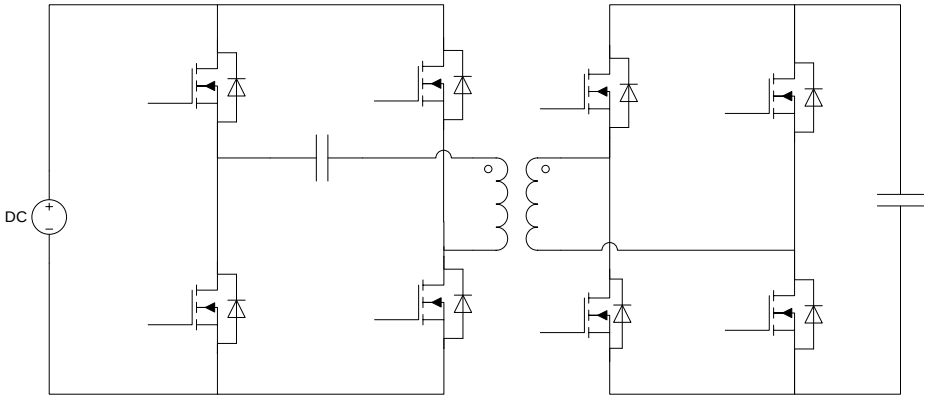

(b)

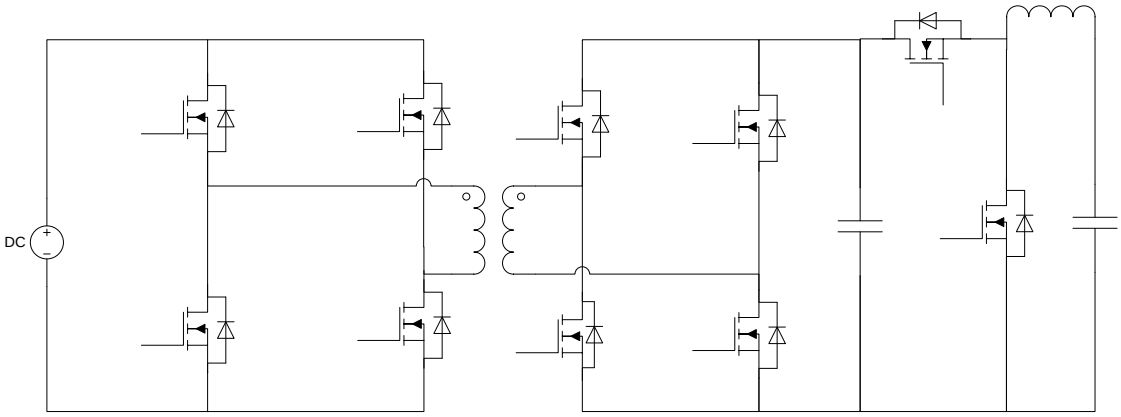

(c)

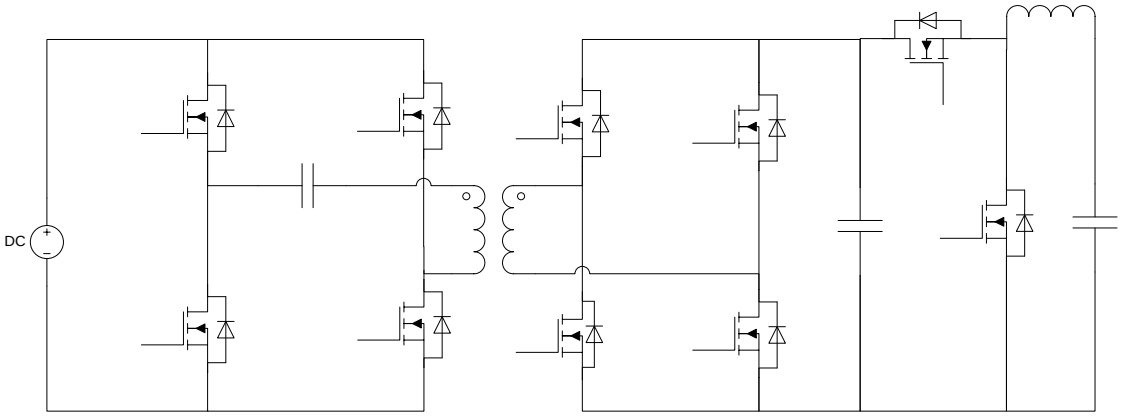

(d)

Fig. 1.9: Several topologies of the full-bridge isolated dc/dc converter

High switching frequency is attractive in reducing the transformer size. However, with increased switching frequency, the switching loss also increases, thus decreasing the overall efficiency. Thus, the resonant circuit in Figures 1.9(b) [19, 20] is introduced to achieve soft switching in these high switching frequency operations, reducing the switching losses and improving overall efficiency. The inclusion of the resonant circuit has the drawbacks of forming a larger converter with more components and higher cost. The voltage regulator at the output voltage in Figure 1.9(c) is useful in operations where "the requirement for the converter to be operated within a wide input and output voltage range results in operation regions of inefficient switch and transformer utilization." The voltage regulator will help in this wide range of voltage at the cost of having extra components, leading to larger converter size and higher cost. In the application of interest, the high voltage bus is a constant voltage, thus a voltage regulator is not necessary. However, the benefits from the resonant circuit block are still considered.

Another implementation of the isolated bi-directional dc/dc converter includes an additional H bridge attached to the end of the high side of a full-bridge circuit can convert the power from dc to ac. This simplifies the overall system structure which requires an inverter to operate. However, for the purpose of this thesis, the inclusion of the additional H bridge can be used as a future addition [21].

In another study [22 - 24], the converter has three bridge legs instead of two for use of a three-port, three phase topology. Although this topology is beneficial to efficiently handle higher power, this operation is more costly than beneficial with the desired power level of 1 kW. Therefore, a standard full-bridge bi-directional converter

topology is best for the target if the thesis which converts dc to dc at 1 kW applications [22 - 24].

Due to the highly attractive advantages of the full-bridge converter, there have been many efforts to alleviate the start-up problem. The most popular solutions are either with magnetics or an active clamp branch. With magnetics, the resonant tank is added in between the high and low side bridges [25, 26]. These resonant tanks are more complex than the capacitor shown in Figure 1.9(b). The magnetic strategy uses switching frequency control which reduces the gain during start-up switching frequency and returns to normal gain during steady state switching frequency. This means the use of frequency controlled gating signals is a lot more efficient compared to using snubber circuits. The drawbacks of the strategy are the increased converter size and cost with the inclusion of the extra resonant block. Additionally, the wide range of frequencies the components in the converter must be operational in leads to costlier and more complex components [27, 28]. Another solution is the inclusion of a flyback snubber circuit. The flyback snubber circuit does not require the resonant tank and frequency controlled gating. However, the snubber circuit decreases the overall efficiency which is important for the purpose of this thesis [29].

Although primarily used to achieve soft switching, the active clamp switch can be combined with the full-bridge switches to help eliminate the start-up problem. Most active clamp circuits involve an extra switching device that is attached to the capacitor preceding the bridge. The input supply can be current-fed or voltage-fed, with an additional input inductor for the system to be current-fed for a unique switching control [30, 31]. The active clamping helps limit the in-rush current as well as the transient

voltage spike which results from control and synchronization between the active clamp and the rest of the circuit. An active clamp can even be combined with the resonant tank; however, this is not necessary for the purpose of this converter [32]. The additional clamping capacitor and switching device introduce additional switching loss and cost, but the control is easier because the system is no longer frequency dependent. This type of topology, shown in Figure 1.10, is a very common topology and has been used in many different studies [33 - 36].

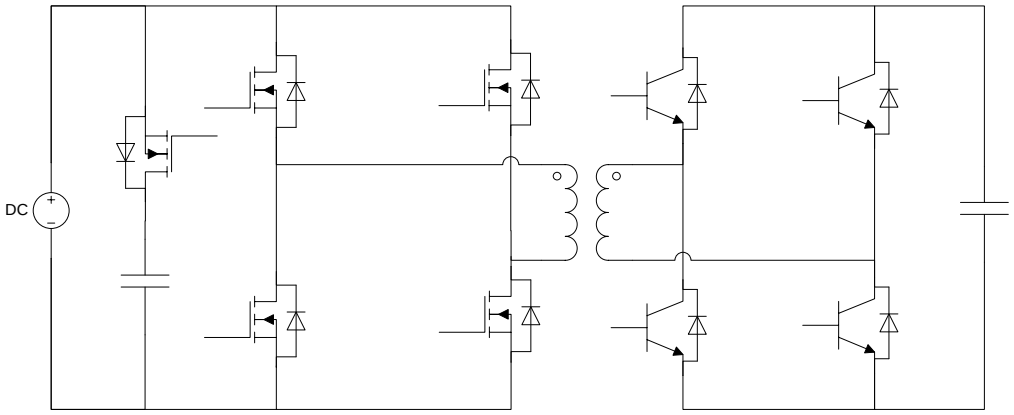

Fig. 1.10: Bi-directional dc/dc converter with active clamp

The experiment of K. Wang uses an active clamp full-bridge isolated bi-directional dc/dc converter, similar to the topologies discussed above. This converter uses the active clamp to limit the transient problems and steady state operations. In the start-up stage of the boost mode operations, the converter uses the flyback transformer to power up the high voltage side bus. After the high side voltage is higher than the low side voltage, the converter operates in normal boost mode operation and the flyback transformer functions as a simple inductor. The addition of the flyback transformer reduces the amount of time to power up the high side load because the power is flowing through the main transformer as well as the flyback transformer instead of just the main

transformer. The diode connected the low side to the high side ensures that current does not flow through the flyback transformer in buck mode operations. In this mode, the flyback transformer also simply functions like an inductor. This proposed converter has a current-fed low voltage side and a voltage-fed high voltage side. Having the low voltage side be current-fed lowers the required turns ratio and reduces the leakage of the transformer, which leads to transient high side voltage. With low switching frequency, the switching losses are reduced, though at a cost of a larger transformer size. Moreover, a duty cycle instead of frequency controlled converter operating at low switching frequency means that the resonant block is no longer necessary for this operation. The drawback is that the inclusion of the active clamp branch along with the flyback transformer requires a larger and costlier converter. Figure 1.11 shows the circuit schematics of the active clamp isolated bi-directional dc/dc converter [14, 37].

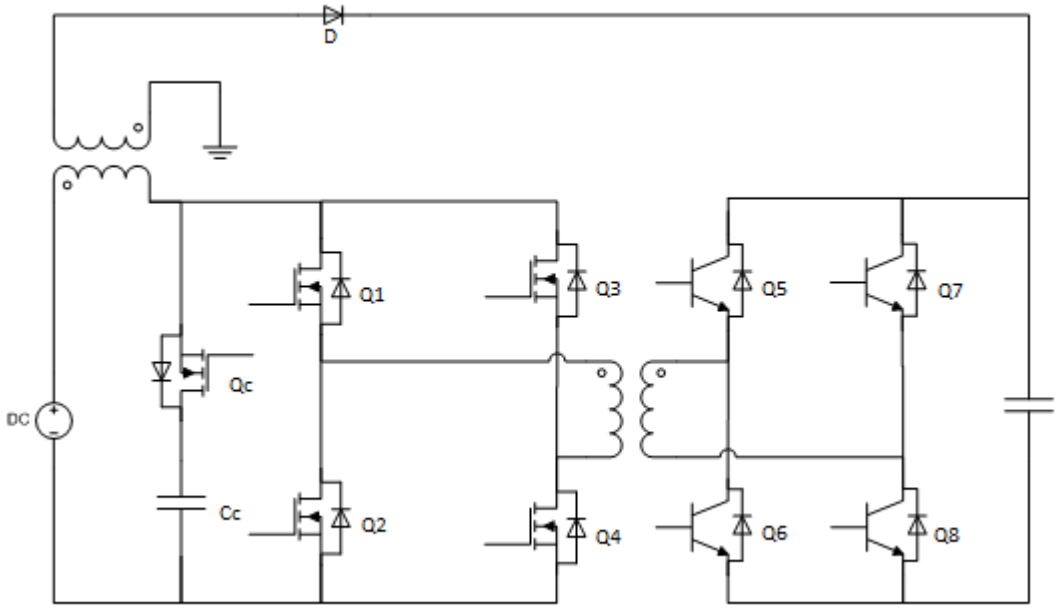

Fig. 1.11: Isolated bi-directional dc/dc converter with active clamp

1.4.3 Hybrid Topology

A hybrid topology which uses the half-bridge and full-bridge is the L-type half-bridge and full-bridge converter as illustrated in Figure 1.12 [38]. This topology has low side L-type half-bridge that is current-fed and high side full-bridge that is voltage-fed. The figure shows the converter with a passive clamp. Although active clamp here is also possible, two separate clamping switches are required for operation [38]. This converter topology has less components than the full-bridge topology overall, but more passive components. Although cheaper to implement, the efficiency of the L-type half-bridge converter is not as high as the full-bridge converter (peak 94% full-bridge, 89% L-type charging; 95% full-bridge, 90% L-type discharging) [38].

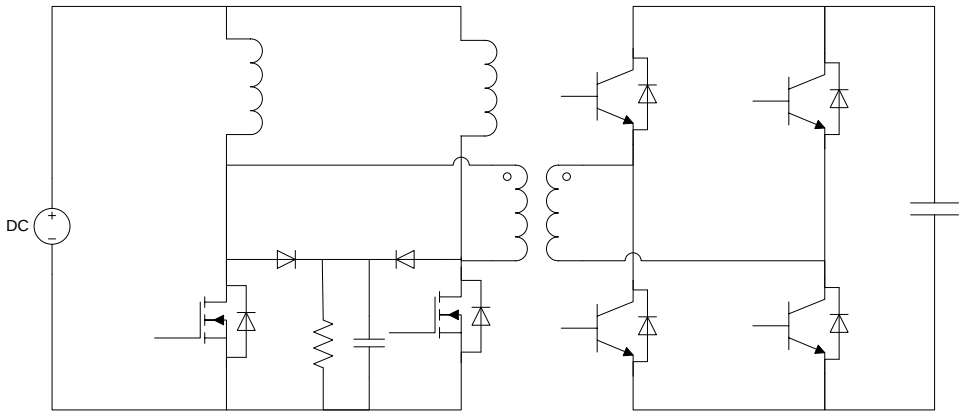

Fig. 1.12: L-type low side full-bridge high side topology

Figure 1.12 shows the use of inductors instead of capacitors on the primary side. This L-type low side full-bridge high side topology also includes the passive clamping circuit of R_C and C_C to improve transients caused by the transformer leakage L_{lk} [39,40].

1.4.4 Topology Selection

After reviewing and comparing several general topologies, it is concluded that there must be active switches on both sides of a transformer for the bi-directional transfer of energy. The transformer is needed for isolation and cases where the low side voltage is significantly different than the high side voltage. To satisfy the conditions of a 48 V to 400 V 1000 W bi-directional converter, the full-bridge topology is most appropriate with its high efficiency and ability to handle high power. A common problem with the full-bridge converter is the in-rush current when the converter is operating in boost mode. This high in-rush current is caused by the uncharged high side capacitor which can destroy components in the circuit. To solve this problem, the full-bridge converter with active clamp is selected. The size restriction of the converter is not a necessity here so low switching operation with the larger transformer and low switching loss is optimal. The extra space taken by the flyback transformer is also insignificant. The low switching frequency also means that the resonant block is not necessary. Lastly, the active clamp branch helps the transient and the start-up time of the converter effectively. The full-bridge converter with active clamp is similar to K. Wang's converter, but with an additional transitional control stage for a more smooth start-up. The extra stage significantly limits current spikes in the start-up stage for full-bridge active clamp converters without any additional components. Therefore, more appropriate components can be used instead of costly large high-current handling parts specifically for the start-up current spikes.

1.5 Thesis Outline

To effectively use renewable energy for clean energy consumption, the transformation of solar energy into electrical energy is a very popular topic. As such, there are several additional goals that must be met for this thesis along with the designing, building, and testing of a bi-directional dc/dc converter. First, a popular voltage level for the standard home appliances dc bus is 400 V dc, and a popular voltage level for large rechargeable batteries is 48 V dc. Therefore, this bi-directional converter must be able to charge batteries at 48 V and use the charged batteries to power the 400 V dc bus. The 400 V dc bus is used to power a 240 V ac inverter which is a very common voltage level for residential applications in the United States. Secondly, the power level must be high enough to be easily useable for several home appliances simultaneously, but not high enough to cause potential danger. Thus, the bi-directional converter must be capable of handling 1 kW for both directions of power transfer. Next, galvanic isolation is required between the high and low voltage side to ensure the safe use of this bi-directional converter. In addition, the start-up problem must be solved for safe use of the converter in boost mode. Although the methods proposed by K. Wang [14, 37] for in-rush current suppression is successful for his study (12 V - 288 V), higher voltage levels can increase the transitional current spike in the start-up mode to a devastating degree. Therefore, a new transitional stage is proposed in this thesis to ensure the functionality of full-bridge boost converters in a much wider range of voltage levels. Lastly, the bi-directional converter must be capable of functioning efficiently in steady state modes. The efficiency is important so that as much as possible of the available power is used to charge the batteries or power the loads instead of being wasted in the converter itself.

The six chapters of this thesis describe the research on an improved isolated bi-directional dc/dc converter for residential applications. The following is the overall organization of this document.

The first chapter provides the general background of the bi-directional dc/dc converter. The purpose of this thesis is discussed with the benefits this study can provide. The common topologies are compared and reviewed along with advantages and disadvantages.

In the second chapter presents the basic operating principle of the isolated bi-directional dc/dc converter. The details of how the converter functions in boost and buck mode are discussed.

In the third chapter, the transient stage is analyzed. Here, the in-rush current associated with the full-bridge boost topology is discussed and a solution proposed. The proposed solution is explained in detail and analyzed with computer software to suggest its practicality.

Merely studying established converter topologies is not enough to develop a new converter. Therefore, in the fourth chapter, the implementation of the circuit is evaluated. The converter is designed to work with similar traits as the previous works, but adjustments must be made to satisfy the goals of this thesis. Therefore, the implementations must be taken to make this converter operational.

In the fifth chapter, the designed prototype is tested for functionality, and experimental results are shown and analyzed.

Finally, in the sixth chapter, the conclusions are drawn from the study and potential future work is proposed as well.

CHAPTER 2: Operation Principle

The ideal bi-directional dc/dc converter works as a full-bridge converter with active switches on both sides of the transformer for bi-directional power transfer. First, the full-bridge converter is discussed; next, both the buck and boost modes are described. The boost mode is more complex than buck mode for including both start-up and regular boost mode.

2.1 Full-bridge Operations

In terms of the full-bridge topology, the operation is quite straightforward. The same figure from Chapter 1.4.1 is now used again to demonstrate the full-bridge topology in Figure 2.1. As the figure shows, there are four active switches which make an ac signal that is carried to the transformer T, the signal is transformed on the secondary side and then rectified by the four diodes into a dc signal again.

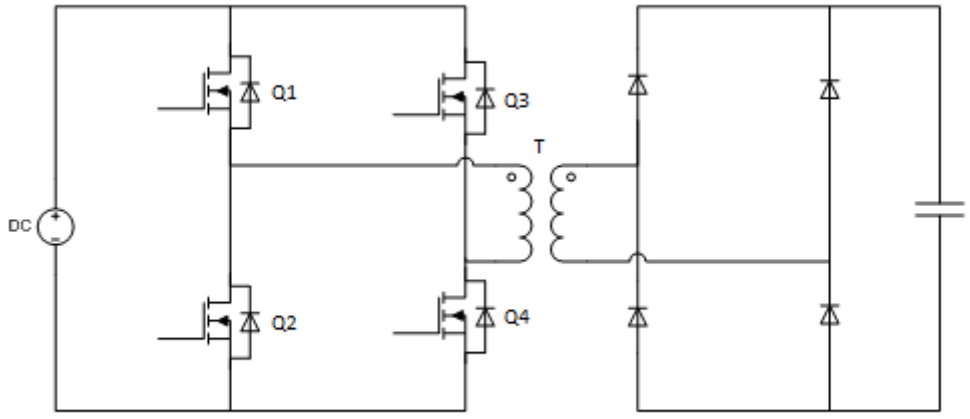

Fig. 2.1: Full-bridge schematics

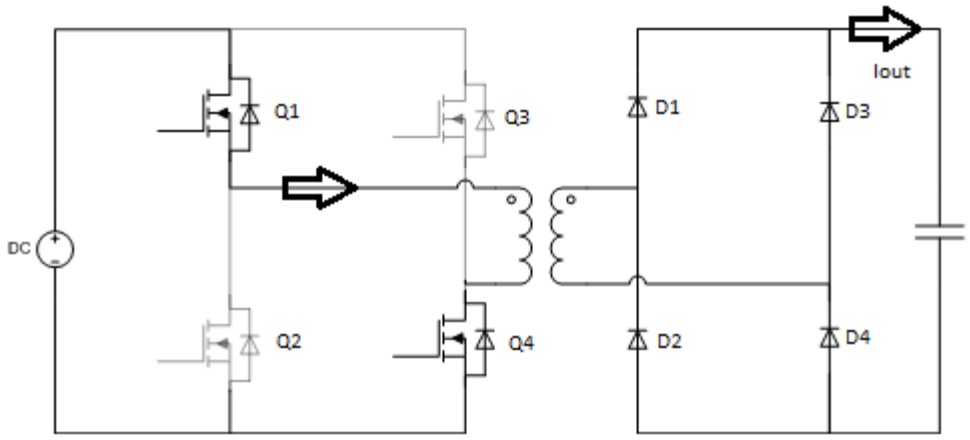

Fig. 2.2: First stage of full-bridge topology

There are two different stages in the phase shift topology; in the first stage, Q1 and Q4 are on while Q2 and Q3 are off. In this stage (illustrated in Figure 2.2), the current is flowing from Q1 into Q4 and thus into the positive terminal of the transformer and out of the negative terminal. Here, the current is flowing in the positive direction.

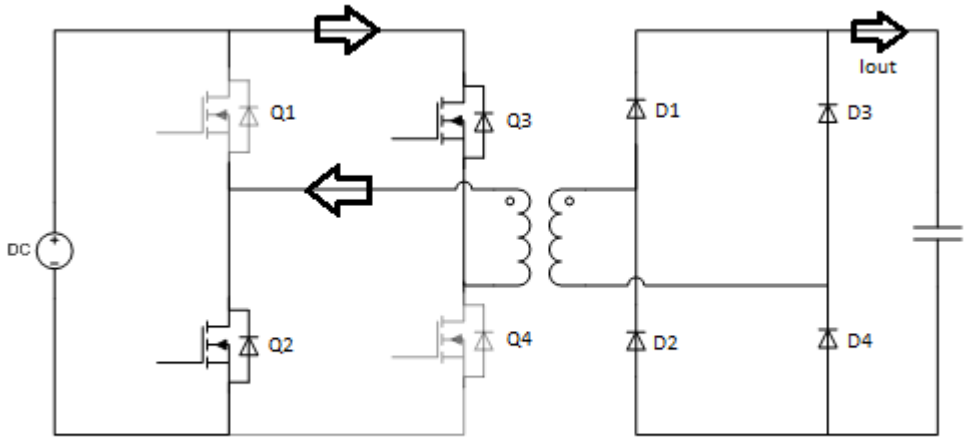

Fig. 2.3: Second stage of full-bridge topology

In the second stage (illustrated in Figure 2.3), Q2 and Q3 are on while Q1 and Q4 are off. The current is now flowing from Q3 to Q2, thus into the negative terminal of the

transformer and out of the positive terminal. Here, the current is flowing in the negative direction.

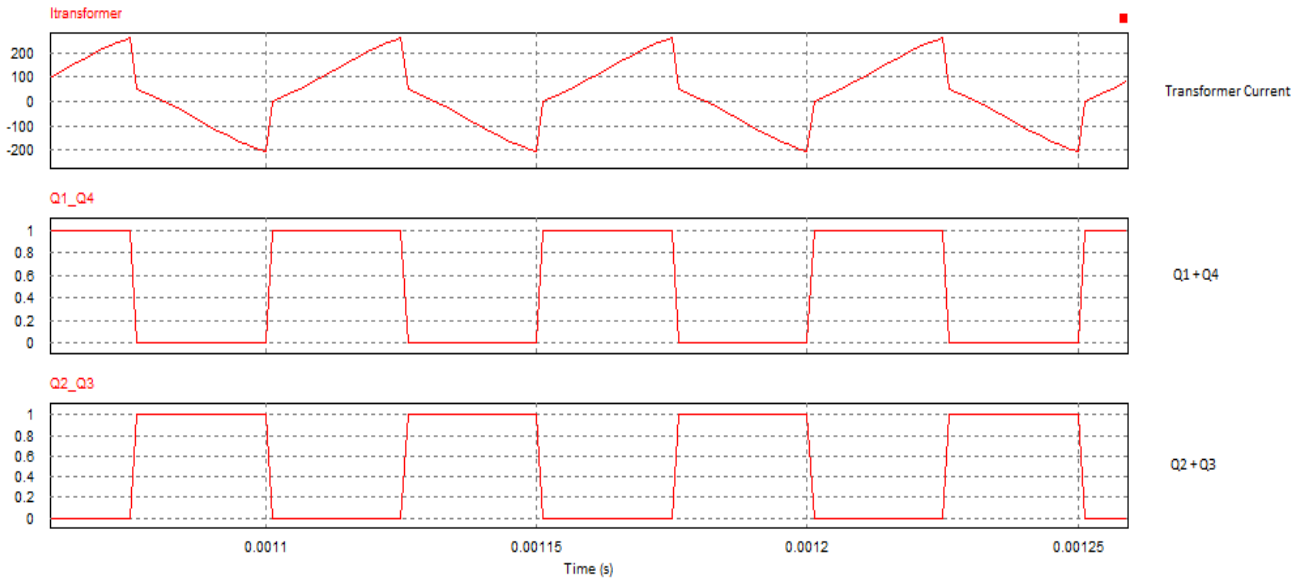

Fig 2.4: Transformer current with respect to switches Q1-Q4 gating

As can be seen in Figure 2.4, the current flowing through the transformer is positive when Q1 and Q4 are on, and negative when Q2 and Q3 are on. The current through the transformer is not a constant dc signal but an ac signal. The ac current is then rectified on the secondary side by the four diodes. With the positioning of the diodes, whether the current is positive or negative with respect to the transformer, it becomes positive with respect to the output. The output then becomes the sum of these currents which forms a constant dc current.

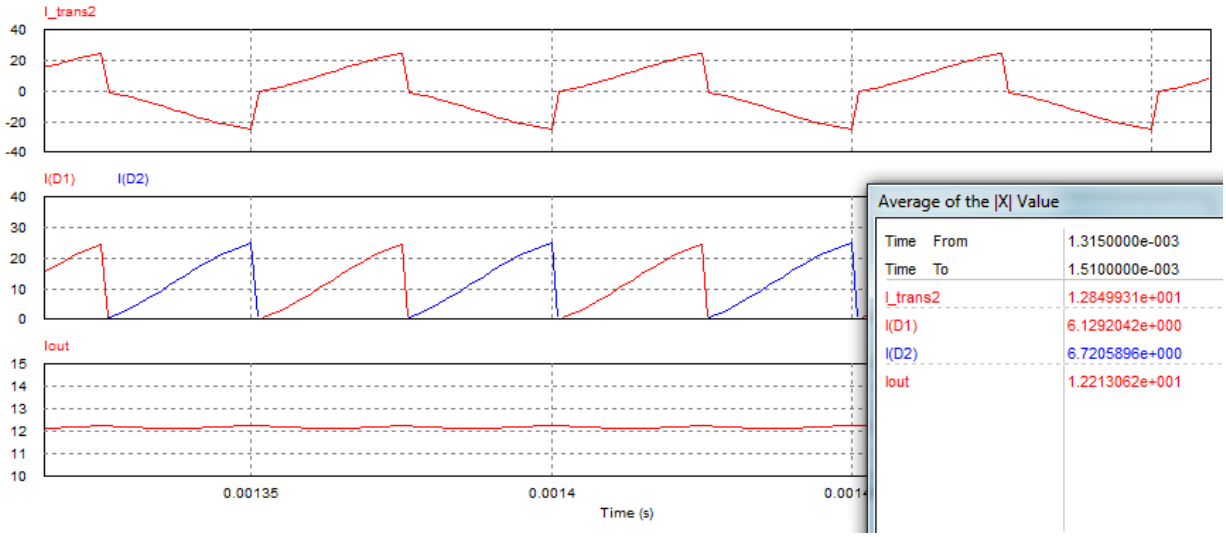

Fig. 2.5: Output current, diodes D1-D4 currents, and transformer current

As Figure 2.5 illustrates, after the diode network on the secondary side, the current flowing to the load is only positive instead of the ac current through the transformer. This is because the four diodes rectifier network will only allow positive current to flow through. After the rectifier network the output current is the sum of the diode average currents and becomes a dc constant current.

The transformer can be used either to amplify or reduce the current flowing through its primary side and secondary side. The turns ratio (n) is used to determine how much the current should be amplified or reduced; the equation for the primary and secondary transformer current is:

$$I_{primary} = n * I_{secondary}$$

2.2 Buck Direction Operations

During the day when the PV panels are absorbing solar energy to convert to electric energy, the energy will be flowing from high voltage side to low voltage side

(buck mode). During this stage, the batteries on the low side are charging. The gates of the high voltage side transistors (Q5-Q8) are controlled according to regular full-bridge mode whereas the gates of the low voltage side transistors (Qc, Q1-Q4) are all off and function as anti-parallel diodes. Figure 2.6 shows the buck operation with the selected bi-directional dc/dc converter topology.

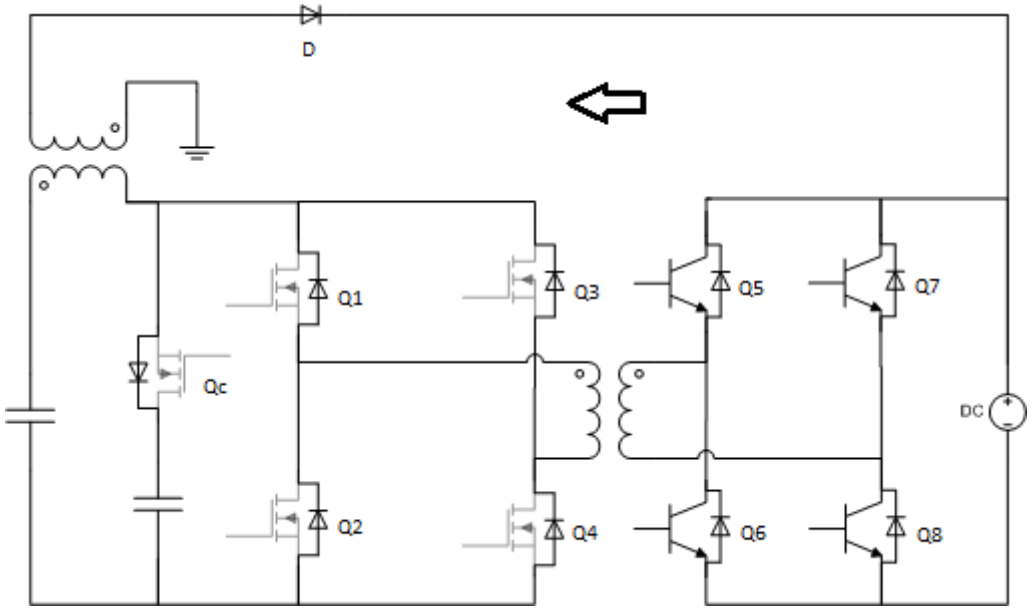

Fig. 2.6: Bi-directional dc/dc converter in buck mode

The arrow in Figure 2.6 indicates the direction of power flow. The diode (D) connecting from the flyback transformer to the output is blocking any current from flowing through, thus the flyback transformer is functioning only as an inductor. The current is not flowing through the clamping switch because the output load has much less impedance. Thus, the current will be flowing into the output and so the clamping switch and capacitor can be ignored as well.

The gating control operates exactly the same as the regular full-bridge converter discussed in Chapter 2.1. In addition, some dead time must be introduced to ensure that shoot through is prevented and zero voltage switching (ZVS) is achieved.

2.3 Boost Direction Operations

When the PV is no longer able to provide energy to the loads, the batteries must be able to transfer energy from low to high voltage (boost mode). In boost mode operations, the high side switches (Q5-8) are now all off and functioning as diodes whereas the low side switches are active. Figure 2.7 shows the schematics of the converter in boost mode operations.

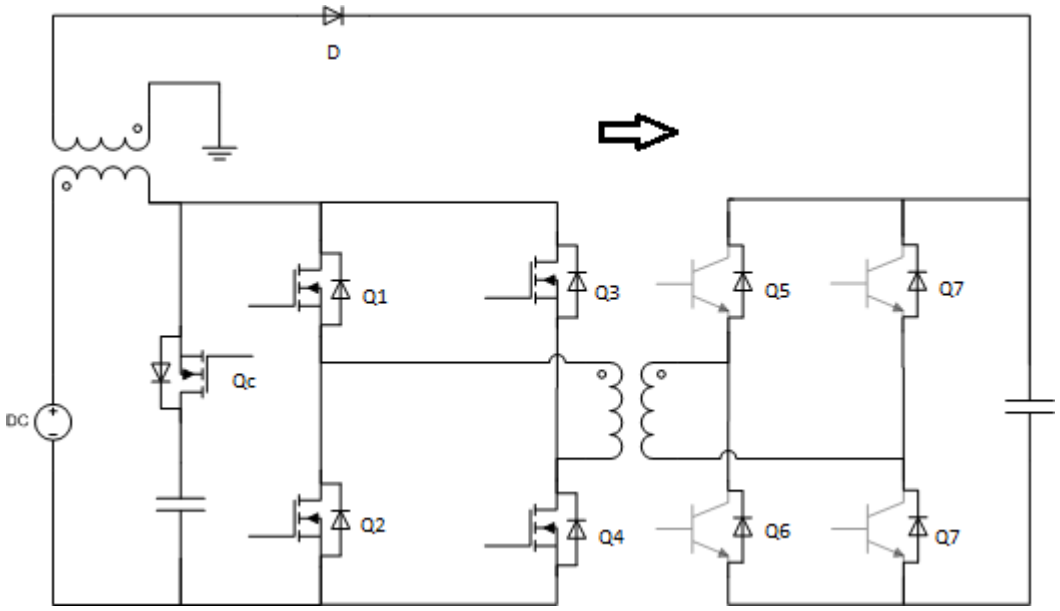

Fig. 2.7: Bi-directional dc/dc converter in boost mode

During boost mode, the high side capacitor is initially at zero voltage, and, thus, the low side sees a short circuit, thereby causing a very high initial current spike. In order for this converter to function, a start-up mode must be introduced.

2.3.1 Start-up Mode

The start-up mode takes place before the converter functions in boost mode to safely charge the output capacitor so when the converter operates in boost mode the initial current spike problem is eliminated. Kunrong Wang [14, 37] introduces a start-up method which solves the start-up problem. In the start-up mode, the converter actually functions as a buck converter, and the energy is transferred to the output with both the forward-flyback transformer as well as the main transformer. The gating signals for start-up and boost mode is shown in Figure 2.8.

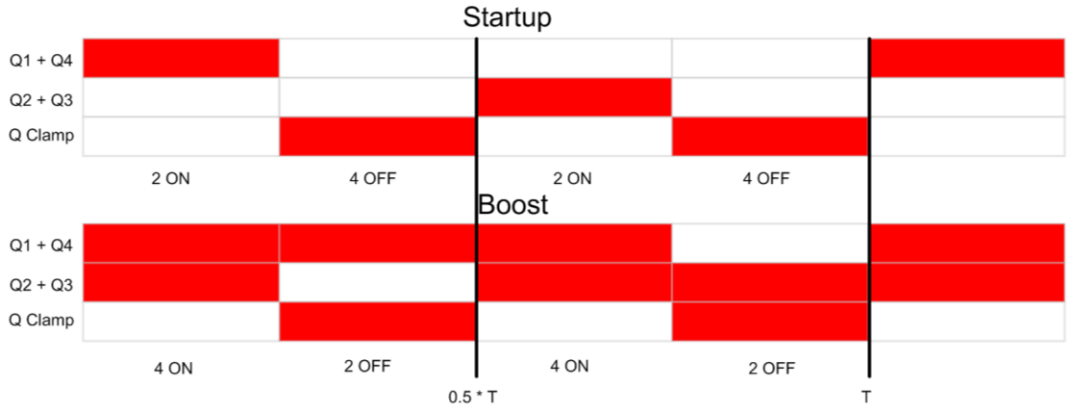

Fig. 2.8: Gating signals for start-up and boost mode for Q1-Q4, Qc

As Figure 2.8 shows, in the start-up stage the duty cycle is less than 0.5, and the converter automatically transitions to boost mode when the duty cycle becomes greater than 0.5. When the duty is very small, the duty of the clamping switch (Qc) is almost 1. As the duty cycle increases, the clamping switch's duty cycle decreases eventually becoming 0 when the main switches (Q1-Q4) reaches duty cycle of 0.5. During the start-up mode there are 2 different stages, the 2 ON stage and the 4 OFF stage.

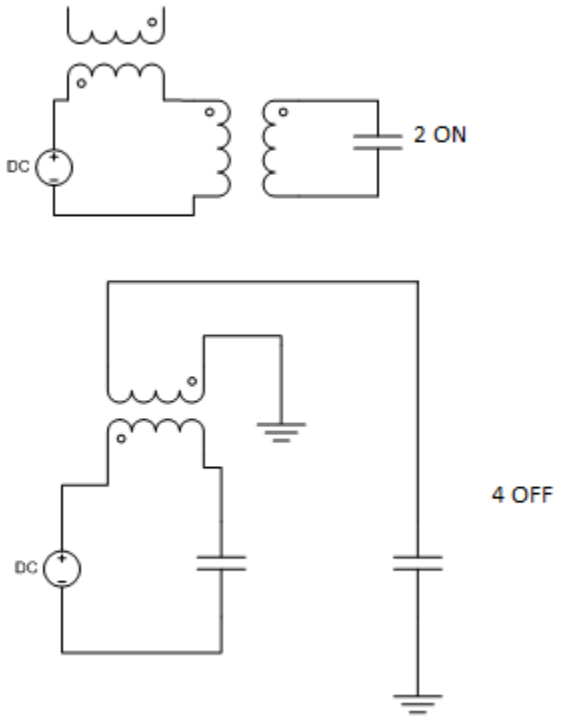

Fig 2.9: Start-up stages schematics

Figure 2.9 shows the schematics of the stages in start-up mode. In the 2 ON stage, either Q1 + Q4 or Q2 + Q3 are on. During this stage, some energy transfers to the output capacitor though the main transformer, and some energy is stored into the flyback transformer's primary side inductor. During the 4 OFF stage, switches Q1-Q4 turns off, the clamping switch turns on and the stored energy in the inductor transfers to the output through the flyback transformer. The equation for the output voltage with respect to the input voltage, turns ratios, and duty cycle is:

$$V_o = \frac{2D}{\frac{1}{n_f} + \left(\frac{1}{n_t} - \frac{1}{n_f}\right) * 2D} * V_i$$

Here, V_o is the output voltage, D is the duty cycle, n_f is the flyback transformer turns ratio, n_t is the main transformer turns ratio, and V_i is the input voltage.

If n_f is set to be the same as n_t (selected to be 8 in this thesis), the equation simplifies to be:

$$V_o = 2D * n_f * V_i$$

2.3.2 Boost Mode

When the duty cycle reaches 0.5, the output capacitor already has voltage across it that is at least the same as the input voltage and boost mode can safely take place. As Figure 2.8 shows, the duty cycle of the clamping switch is 1 when the main switches duty cycle is 0.5, then decreases as the main switches' duty cycle increases. In boost mode, there's also 2 stages that take place, the 4 ON stage and the 2 OFF stage. The schematics of the circuit are shown for both these 2 stages in Figure 2.10.

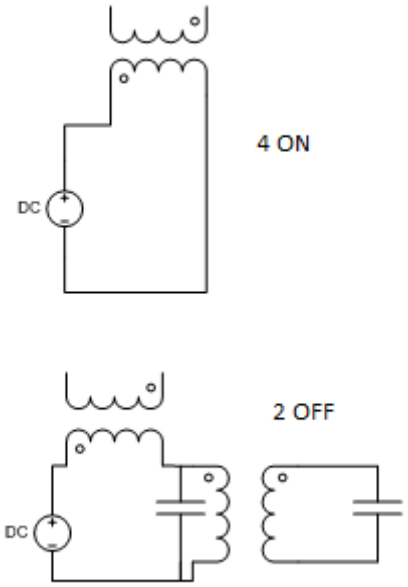

Fig. 2.10: Boost stages schematics

As Figure 2.10 illustrates, during the 4 ON stage, all 4 switches are on and the flyback transformer (now operating as an inductor) charges. During the 2 OFF stage, the

energy releases into the output through the main transformer. Note that in boost mode, the flyback transformer is only functions as an inductor and there is no longer any current flowing into the output from it. The equation for the output voltage with respect to the input voltage, transformer turns ratio, and duty cycle is:

$$V_o = \frac{1}{2-2D} * n_t * V_i$$

With the start-up connected to boost mode, the converter is able to avoid the high initial current spike [41].

2.4 New Problem Introduced

Although the initial current is reduced, a new problem is introduced by the start-up method that Kunrong Wang developed [14, 37]. The problem occurs when the converter switches from start-up mode to boost mode. When the duty cycle of the main switches get close to 0.5, the clamping switch duty cycle is almost 0, and when the main switches gets to 0.5, the clamping switch duty cycle is almost 1. When the clamping switch duty cycle is approaching 0, the clamping capacitor is being charged up, and when the clamping switch duty becomes 1, the charge on the capacitor is released. The fast change of the duty cycle from 0 to 1 causes a very large current spike which may destroy components. In order for the bi-directional converter to be fully and safely functional, this new problem must be solved. Thus, a new transitional stage between Kunrong Wang's start-up and boost stages is introduced.

CHAPTER 3: Transitional Stage

3.1 Current Spike Analysis

In order to eliminate the detrimental current spike that occurs when the converter switches from start-up to boost mode transition, an additional stage is introduced. In the experimental results of Kunrong Wang [14, 37], the current spike of the transformer reaches as high as about 80 A while the steady state current peak is less than 20 A. Because this current waveform is on the high voltage (low current) side of the transformer, with the turns ratio being 12, the current on the low voltage (high current) side is about 960 A. To verify the presence of this current spike for this bi-directional converter, a PSIM simulation is shown in Figure 3.1.

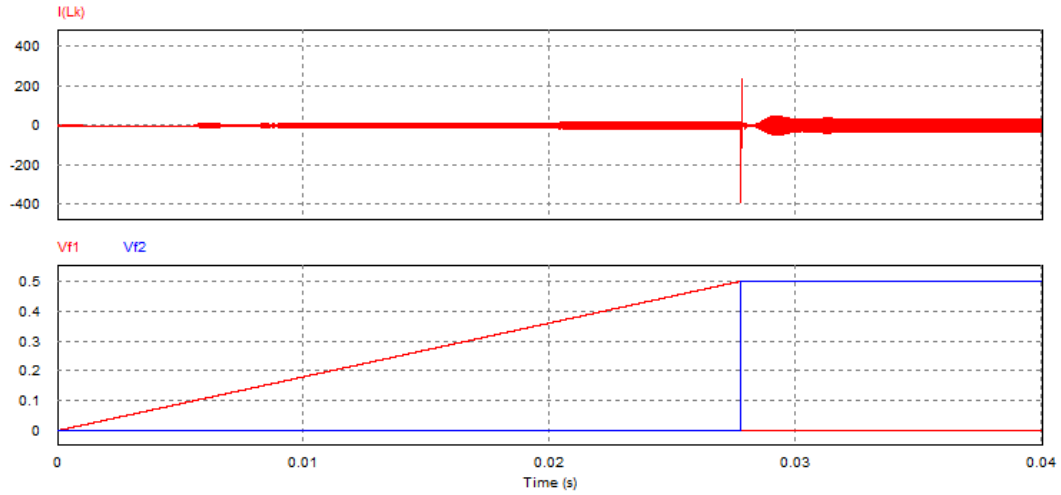

Fig. 3.1: Transformer current vs. duty cycle start-up and boost mode simulations

In Figure 3.1, the Vf1 and Vf2 are the duty cycles of the main bridge switches and I(Lk) is the current through the transformer on the primary side (Fig 2.4). The gating logic of the start-up mode and boost mode mentioned in Section 2.3.1 is used in this

simulation. The start-up mode duty cycle is represented by Vf1 and boost mode is represented by Vf2. In this simulation, boost mode occurs when Vf2 is active. As shown in Figure 3.1, the two gating schemes do not occur simultaneously. The current spike occurs when the duty cycle is at 0.5, precisely when the converter switches to boost mode (Vf2). As the figure illustrates, the in-rush current at the very beginning is eliminated. However, the current spike occurring exactly when the transition of start-up and boost mode is about 400 A which is a devastating problem. This high current spike requires the use of high current handling devices for safe operations. The use of high current handling devices for the brief start-up isn't cost effective when the steady state current is significantly lower. Thus, a method to alleviate the current spike for the use of appropriate devices is desirable.

3.2 Current Spike Solution

To reduce the transitional current spike, the clamping switch's duty cycle must be transitioned gradually from 0 to 1 after the start-up stage. When the main switches approach the duty cycle of 0.5, the clamping switch duty cycle is near 0. At the moment the main switches reach 0.5 duty cycle, the clamping switch duty cycle should slowly increase to 1 instead of jumping straight to 1 to avoid the large current spike.

The proposed transitional stage occurs right before the main switches reach the duty cycle of 0.5. The order for proper operation is start-up, transitional, and normal boost stage. When the transitional stage occurs, the main switches' duty cycle remain at 0.5. The clamping switch's duty cycle increases gradually from 0 to 1 instead of jumping from 0 to 1. During the transitional stage, the output voltage is already be built up, thus the start-up in-rush current does not occur. With the main switches' duty cycle at 0.5, the

converter operates with regular full-bridge operation. Therefore, the power continues to be transferred through the main transformer and not the flyback transformer. The main power path and the output voltage are not affected by the switching of the clamping switch. The transitional stage, like the start-up stage, is very brief and therefore, power losses are insignificant. Figure 3.2 below shows the schematics of the two stages during the transitional stage.

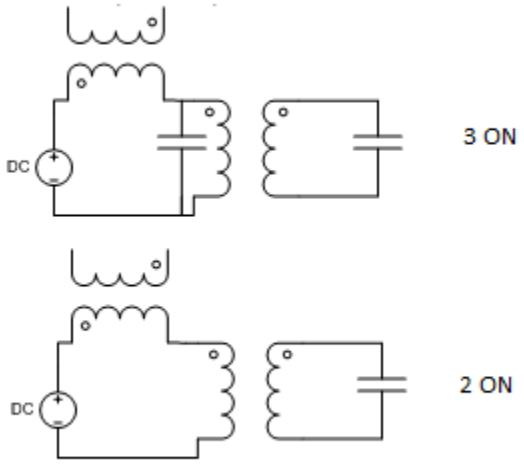

Fig. 3.2: Transitional stage schematics

As shown in Figure 3.2, switching the clamping switch connecting to the clamping capacitor doesn't affect the main power path. The duty cycle of this switch initially is very low, meaning the 2 ON stage is predominate in each switching period. Then, the duty cycle increases leading to the 3 ON stage being majority of each switching period. The purpose of preventing the sudden discharge of the clamping capacitor while not affecting the main power path of the converter is achieved by this proposed transitional stage. The converter is therefore, capable of safely transitioning from start-up to boost mode.

The converter operates in normal boost mode when the duty cycle of the clamping switch increases to 1. The transitional stage ensures a smooth transition from start-up to regular boost with a significantly reduced current spike. Figure 3.3 shows the duty cycles of switches Q1 + Q4, Q2 + Q3, and Qc from start-up mode to steady state boost mode. Here, the switching frequency is much lower than actual applications to be visually clear; the duty cycle of switches Q1 - Q4 in steady state boost mode is arbitrarily selected to 0.55.

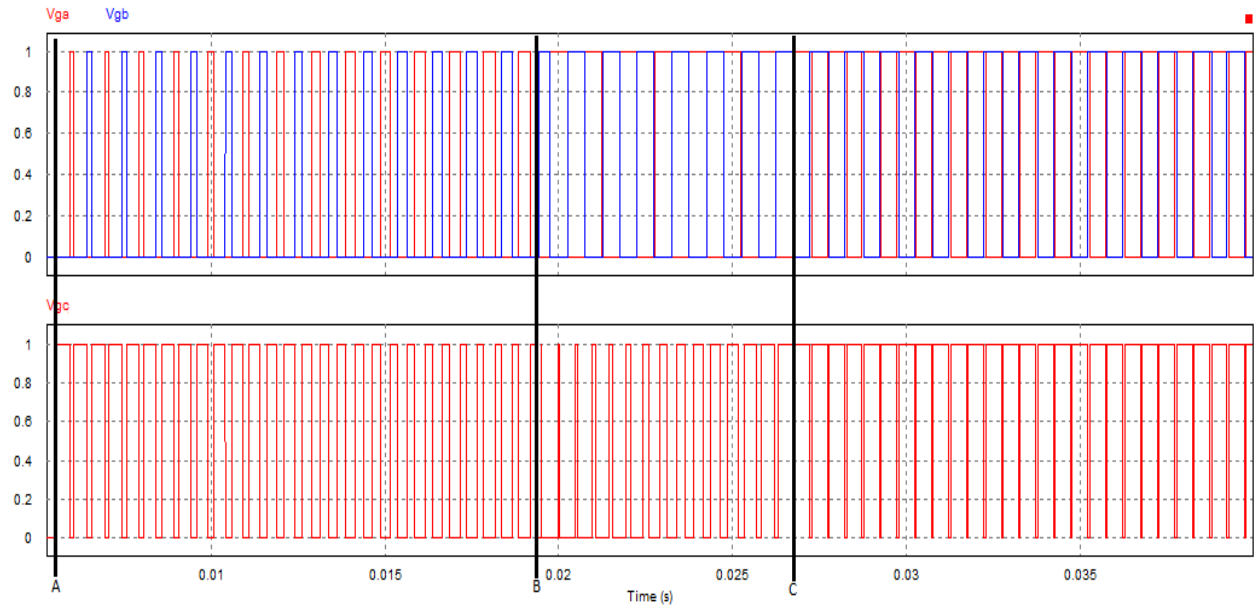

Fig. 3.3: Duty waveforms of switches

The three different stages: start-up (A), transitional (B), and boost (C) is shown in Figure 3.3. In the start-up stage (A), the main bridge switches (Vga and Vgb) starts with low duty cycle which then increases. The clamping switch (Vgc) in contrast starts with high duty cycle which decreases. When the transitional stage is reached, the duty cycle of the clamping switch is 0 and for the main switches is 0.5. During the transitional stage (B), the duty cycle of the main switches remains 0.5 whereas the clamping switch increases from 0 to 1. When the duty cycle of the clamping switch reaches 1, boost mode

(C) takes into effect. In boost mode, there is some overlap of the main switches. During these overlap, the clamping switch is off. Figure 3.4 shows the simulation results of the transformer current.

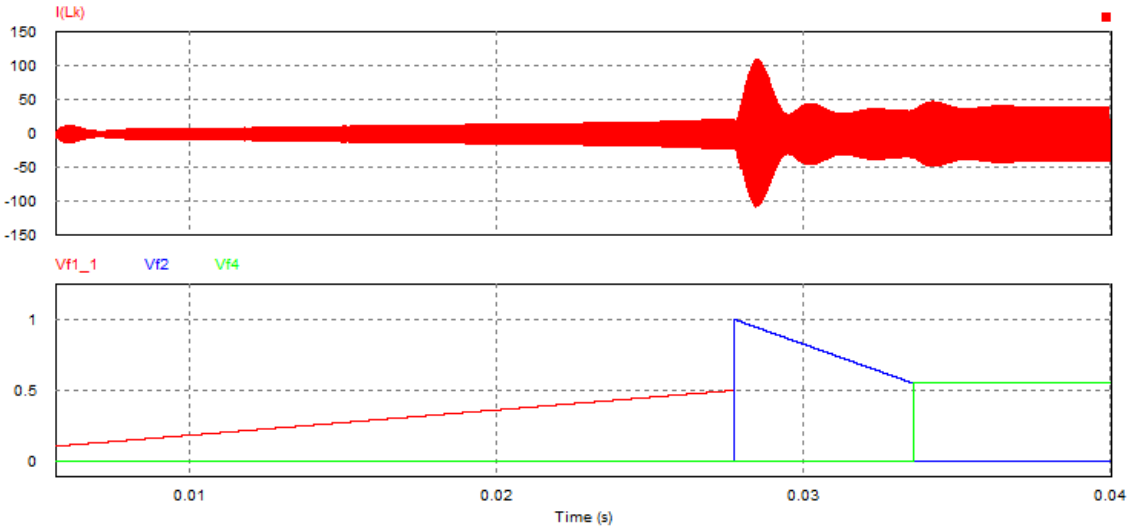

Fig. 3.4: Transformer current vs. duty cycle with transition stage

In Figure 3.4, the duty cycle graph has 3 stages: start-up (red), transitional (blue), and boost (green). In the start-up stage, the duty cycle rises from 0 to 0.5. In the transitional stage, the duty cycle of the clamping switch is 0 in the beginning (in this stage, Vf2 shows the comparator signal that makes the duty cycle of the clamping switch to increase from 0 to 1 as shown in Figure 3.3), then increases (decreases in the graph) until the duty cycle of the clamping switch is 1 where boost mode kicks in. The current spike is now reduced to about 100 A which is much lower in comparison to the 400 A achieved without the transitional stage. Figure 3.5 shows the output voltage and the voltage stress of the clamping switch.

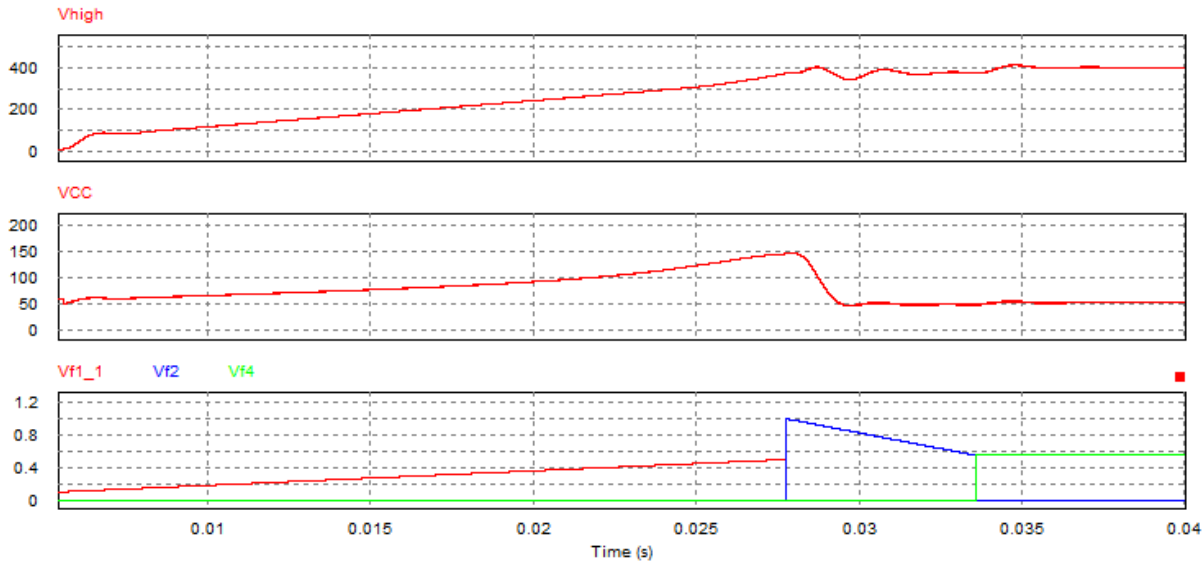

Fig 3.5: Output Voltage vs. voltage stress vs. duty

As Figure 3.5 shows, the voltage stress of the clamping switch (VCC) increases to as high as 150 V when the duty cycle is in the start-up mode. The voltage stress is caused by the charging of the clamping capacitor as the clamping switch duty cycle approaches 0. The output voltage (Vhigh) is capable of smoothly achieve 400 V without any voltage spikes. As shown by the simulation results, the converter is able to safely and smoothly transition from start-up mode to boost mode with the inclusion of the transitional stage.

CHAPTER 4: Implementation

This chapter includes the discussion of implementations for both buck mode and boost mode operations. This converter operates at 1000 W power with 400 V on the high voltage side and 48 V nominal on the low voltage side. This equates to the current being 2.5 A on the high voltage side and 20.83 A on the low voltage side.

4.1 Buck Mode Implementations

4.1.1 Buck Mode System

For buck mode implementations, the battery charging characteristics discussed in Section 1.2 are applied. Because the load of a battery is difficult to model, a simple resistor bank in parallel with a bus capacitor is used. The goal of the bi-directional converter in buck mode is to provide constant current, then constant voltage to the load. Although both the current and the voltage levels are arbitrary, the current is set to 20 A during constant current mode and the voltage at 48 V during constant voltage mode for this specific converter. The overall system of the bi-directional dc/dc converter operating in buck mode is shown in Figure 4.1.

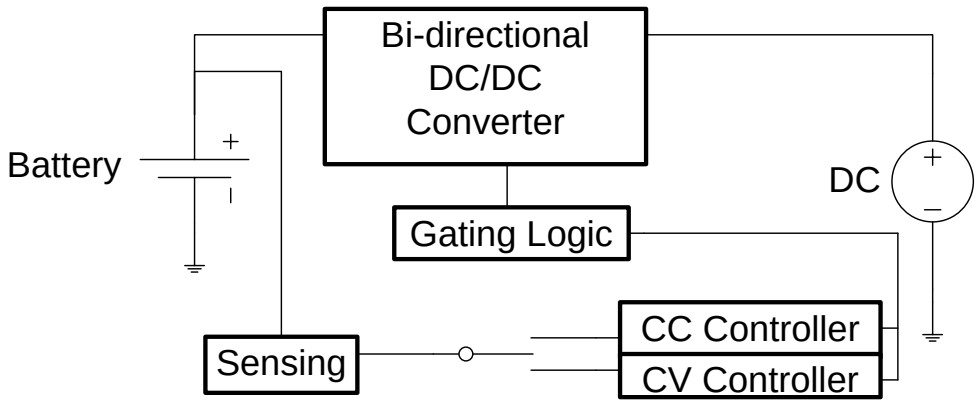

Fig. 4.1: Buck mode system

As Figure 4.1 shows, both current and voltage sensing are required, with only one mode active at any given instance. The transition from CC and CV mode is programmed to occur with the achievement of a predetermined voltage level of the load bank. Ideally, the converter initiates with constant current mode, during which both the voltage and current sensors are actively monitored. When the load bank reaches the predetermined voltage level, CV mode occurs where the voltage sensor is monitored. If the voltage level drops below that threshold, CC mode re-activates to maintain the charge capacity of the battery.

4.1.2 Buck Mode Controllers

Closed loop controllers are designed to maintain system stability during constant current and constant voltage mode. For the purpose of this converter, a proportional integral (PI) controller is appropriate for functionality. Several methods can be used to design the controller such as modeling and calculations, and trial and error. Although trial and error is the easiest method, the process can potentially be time consuming without a good starting point. In contrast, modeling and calculation method can produce accurate and precise controllers. However, these results may require further tuning for

actual experimentations. Thus, the selected method for this converter is to first analyze the frequency response of the system in open loop mode, then select pole(s) and zero(s) in appropriate locations by trial and error to produce a stable system. Simplis is the software selected to simulate the frequency response of the system, the schematics in this software is shown in Figure 4.2.

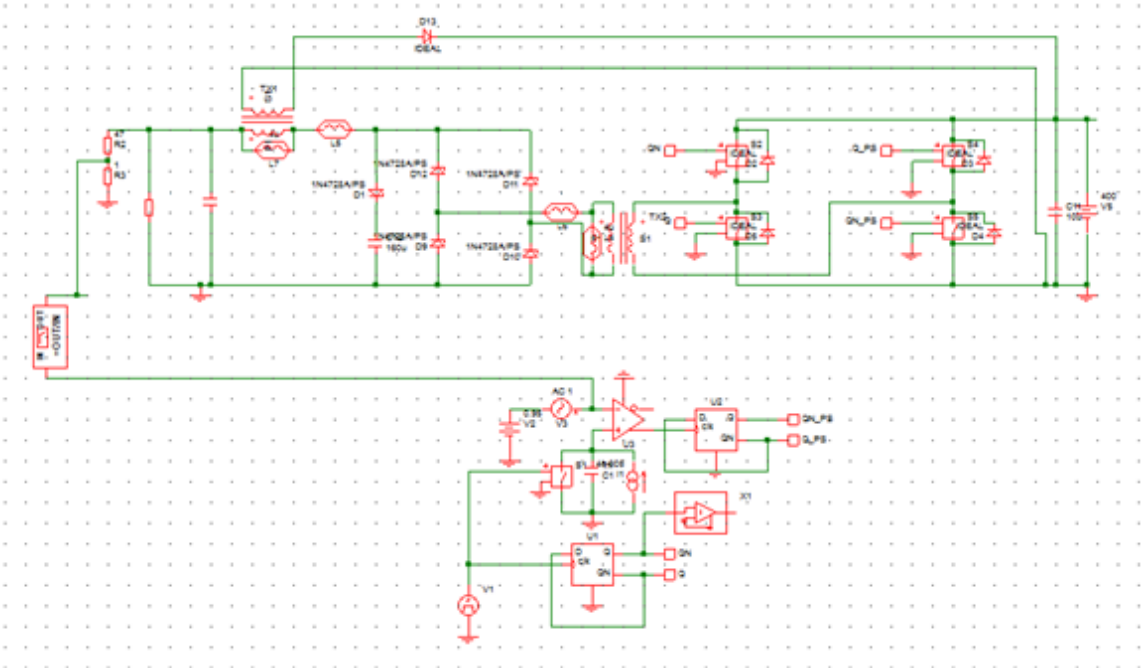

Fig. 4.2: Simplis buck mode schematics

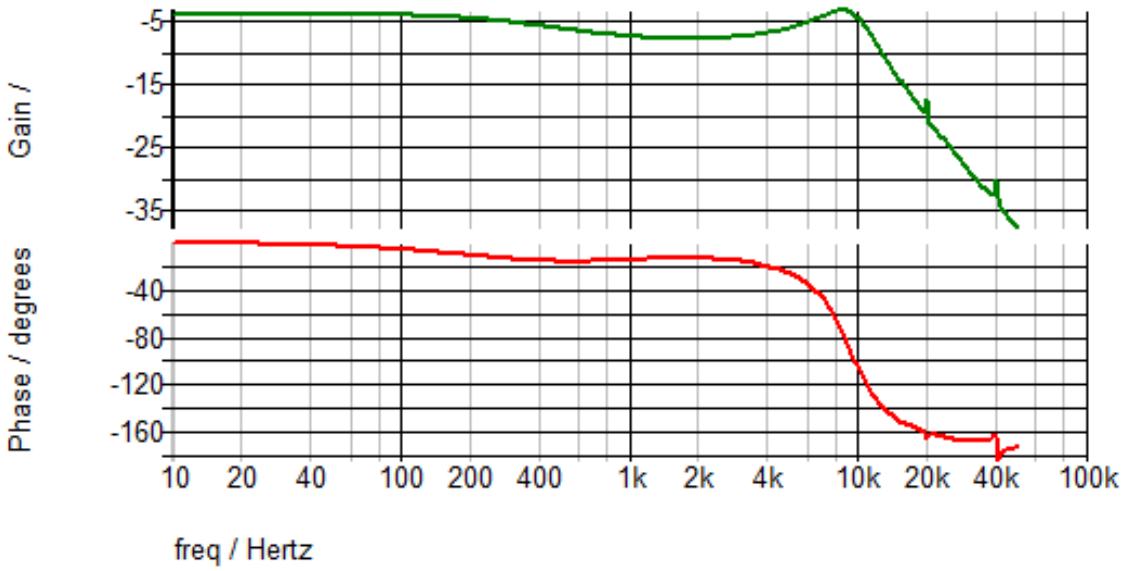

Fig. 4.3: Simplis buck mode simulation results

The simulations result in the bode plots of the system is shown in Figure 4.3. The data from the Bode plots is then imported to MATLAB Sisotool to create a controller for the stability of the system in closed loop. Figure 4.4 shows the same data from Figure 4.3 opened in Sisotool.

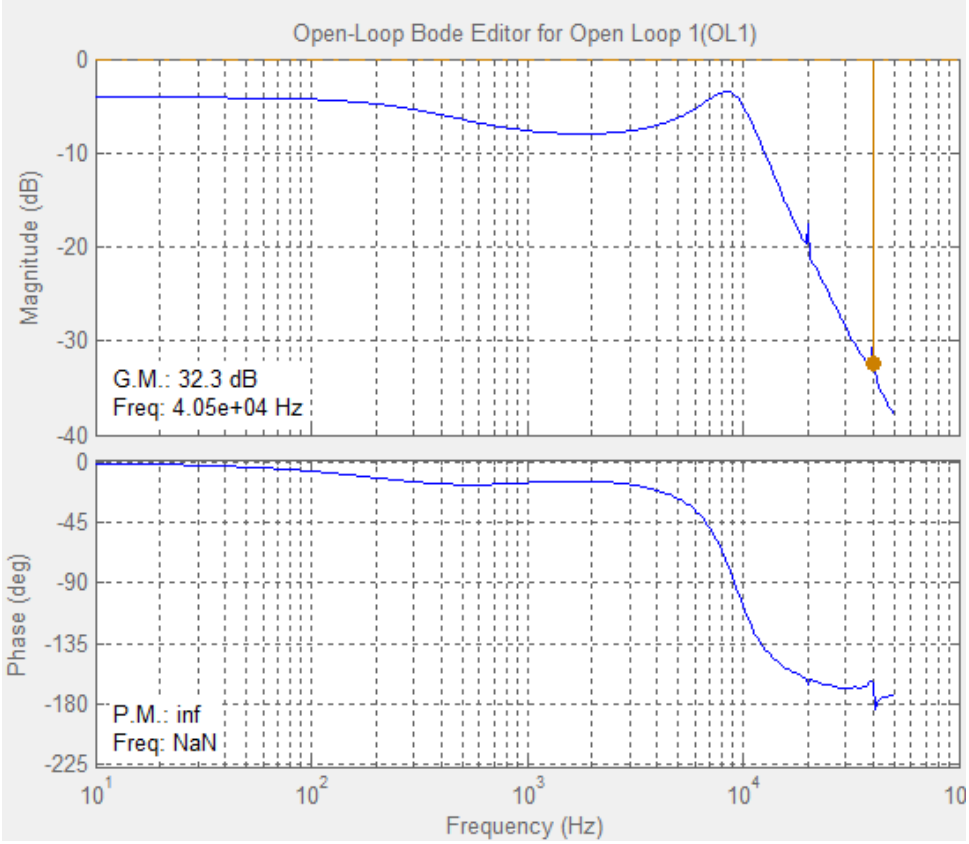

Fig. 4.4: Sisotool for buck mode in open loop

As shown in Figure 4.4, there is no bandwidth or phase margin because the gain is under 0 decibels (dB). The figure also shows a gain margin of 32.3 dB. The goal for a stable system calls for the gain margin to be at least 10 dB, phase margin that is at least 60˚, and bandwidth equal to 2 kHz, an order of magnitude lower than the switching frequency, which is 20 kHz. Figure 4.5 shows the Bode plot with the controller.

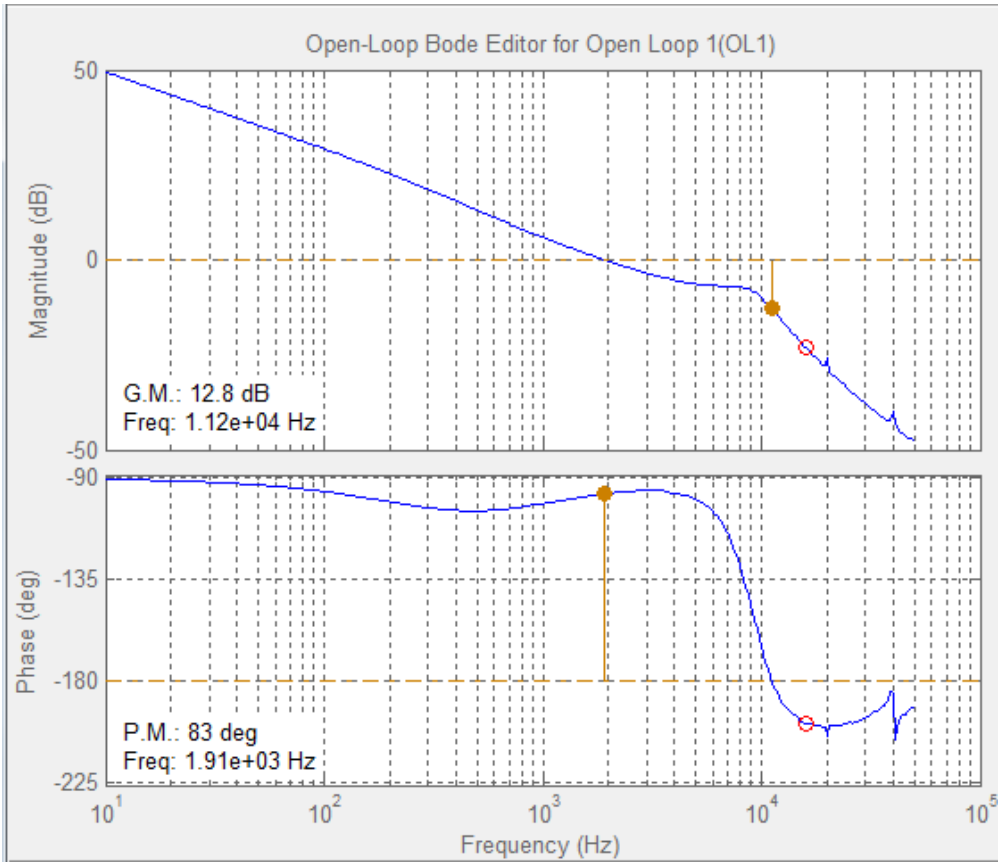

Fig. 4.5: Sisotool for buck mode with controller

As indicated in Figure 4.5, with the inclusion of the controller, the phase margin is now 83˚, gain margin is 12.8 dB, and crossover frequency is equal to 1.91 kHz indicating a stable system with appropriate bandwidth. Sisotool gives out the PI controller transfer function which is produced in PSIM to verify good stability. However, this set of data is trivial since they change when tuning the PI controller in actual experimental applications, and thus not included.

4.1.3 Buck Mode Simulations

To verify the functionality of the battery charging system in buck mode, simulations in PSIM are analyzed. Figure 4.6 shows the schematics of the bi-directional

dc/dc converter in buck mode, where non-ideal parameters (leakage inductance, etc) are included to model real experimental results.

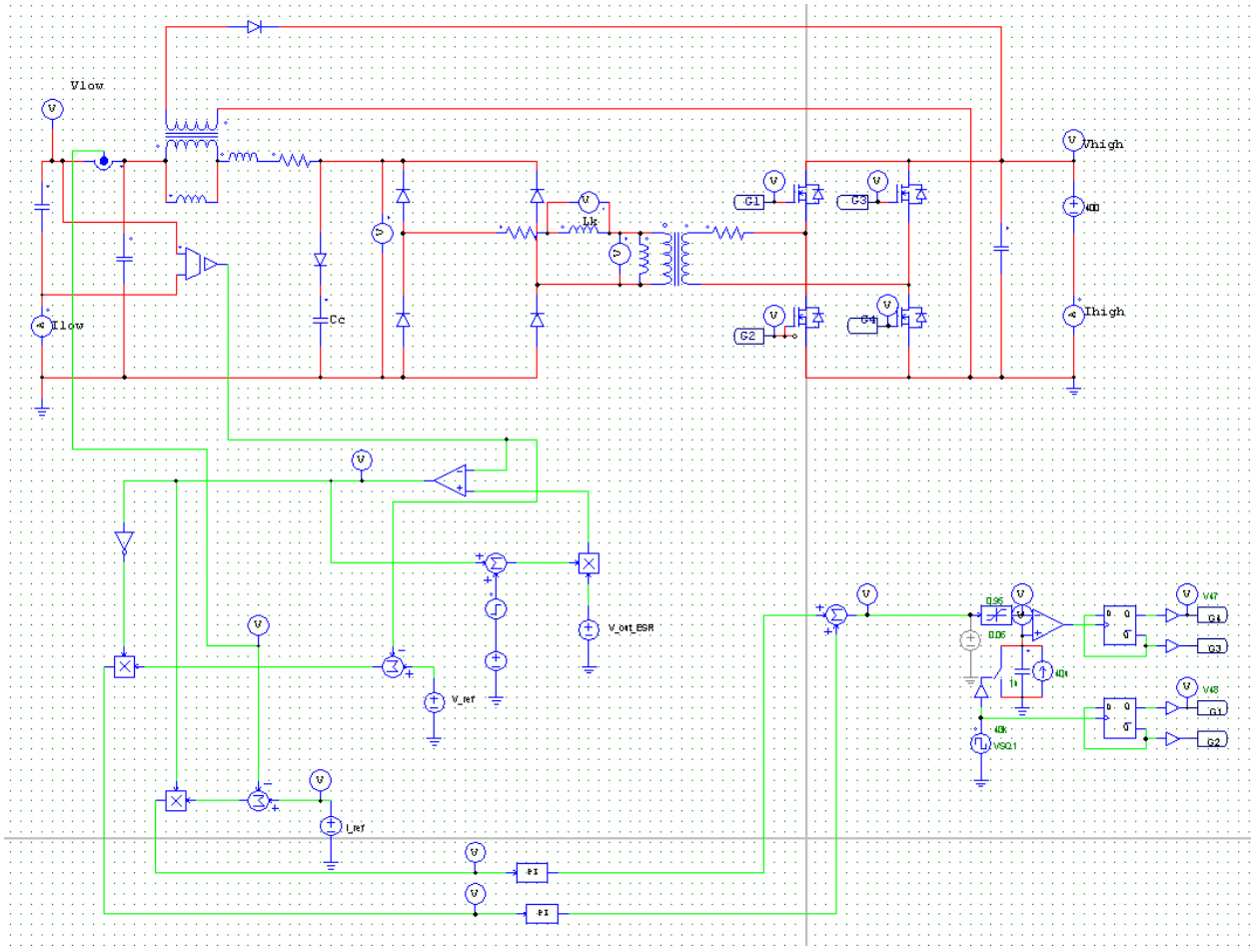

Fig. 4.6: PSIM buck mode schematics

As shown in Figure 4.6, the switches on the low voltage side are off and are represented by diodes. To better see the charging operations of the battery in simulations, a large capacitor represents the output load instead of a resistor. The overall schematics representing the system in Figure 4.6 are shown in Figure 4.1. The logic on the lower left corner of Figure 4.1 is the logic that is used to switch between constant current and current voltage mode. The gating logic circuits on the lower right of Figure 4.6 are used to drive the gates with phase shift control. The two PI controllers on the bottom of this

same figure are the controllers for constant current and constant voltage mode. The PI controllers are exactly the same, however, they may potentially be changed to be compatible with the actual sensing circuitry. Figure 4.7 shows the simulations results of the schematics shown in Figure 4.6.

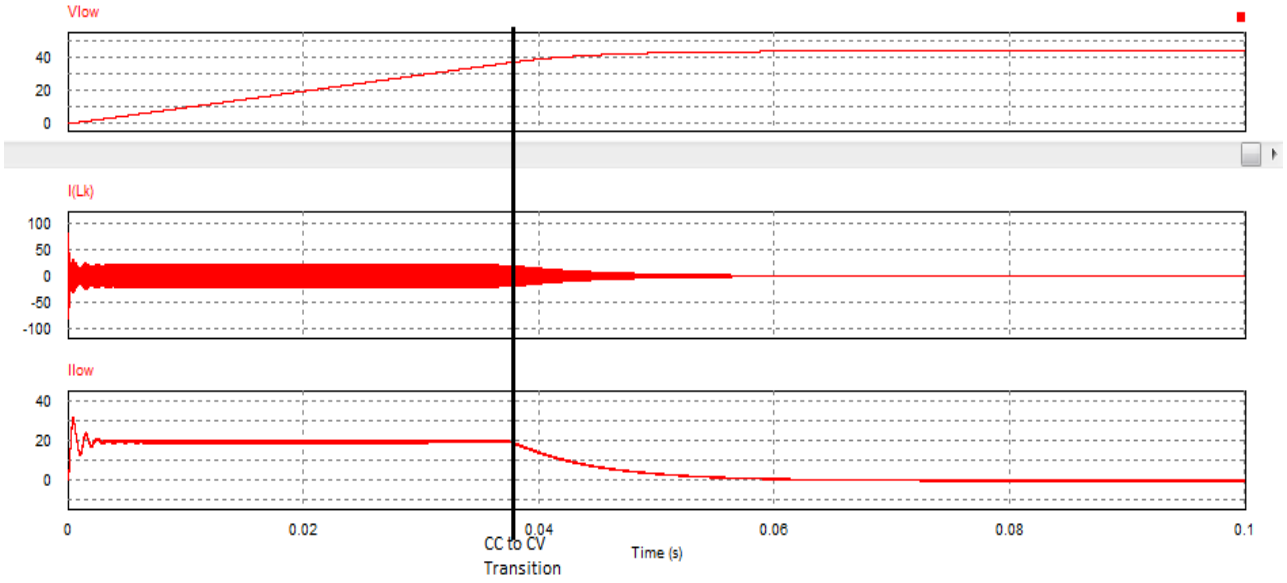

Fig. 4.7: PSIM buck mode simulation results

In Figure 4.7, the output voltage (Vlow), transformer current (I(Lk)) and output current (Ilow) are shown to demonstrate functionality. As the figure suggests, the converter starts with constant current mode operations where the output current is kept steady at 20 A (arbitrarily selected to be near full load current). The output voltage is constantly increasing during this constant current period as the battery is charging. The point at which the transition from constant current to constant voltage occurs is arbitrarily selected to be about 39 V. As the results show, when the transition occurs the output current starts to drop as the output voltage slowly rises to the set voltage reference. From the transformer current graph, it is shown that the initial current spike is in a safe operating region. The output current and transformer current becomes 0 when the battery

is fully charged (here, modeled by the converter reaching voltage reference). The simulation results suggest a functioning isolated bi-directional dc/dc converter in buck mode for battery charging.

4.2 Boost Mode Implementations

The boost mode requires the start-up, transitional, and boost stages for functionality. During start-up and transitional stage, the converter is functioning in open loop with the gating signals programmed prior to experimentation. After the transitional stage, the converter operates in closed loop boost operations. This section describes the implementations of the simulation results for the three stages shown in Chapter 3.

To achieve soft switching for reducing switching losses, the clamping capacitor must be resonant with the leakage inductance. However, since the clamping capacitor can resonate with the main transformer leakage inductance or with the flyback transformer leakage, the selection of the clamping capacitor must be with the worst case. The resonant period must be longer than half of the switching frequency's period. The equation below gives the equation for the clamping capacitor design:

$$C_C \geq \max\left[\frac{1}{16 * L_{Transleakage} * \pi^2 * f_s^2}, \frac{1}{16 * L_{Flybackleakage} * \pi^2 * f_s^2}\right]$$

The equations relates to the transformer ($L_{transleakage}$) and the flyback transformer ($L_{flybackleakage}$), as well as the switching frequency (f_s). With both the flyback transformer as well as the main transformer leakage considered, the clamping capacitor value with the larger capacitance is selected.

4.2.1Boost Mode Controller

When the converter enters regular boost mode, it operates in closed loop operations. For this converter, like in buck mode, a PI controller is appropriate for stable applications. Figure 4.8 shows the Simplis bode plots of the converter in boost mode.

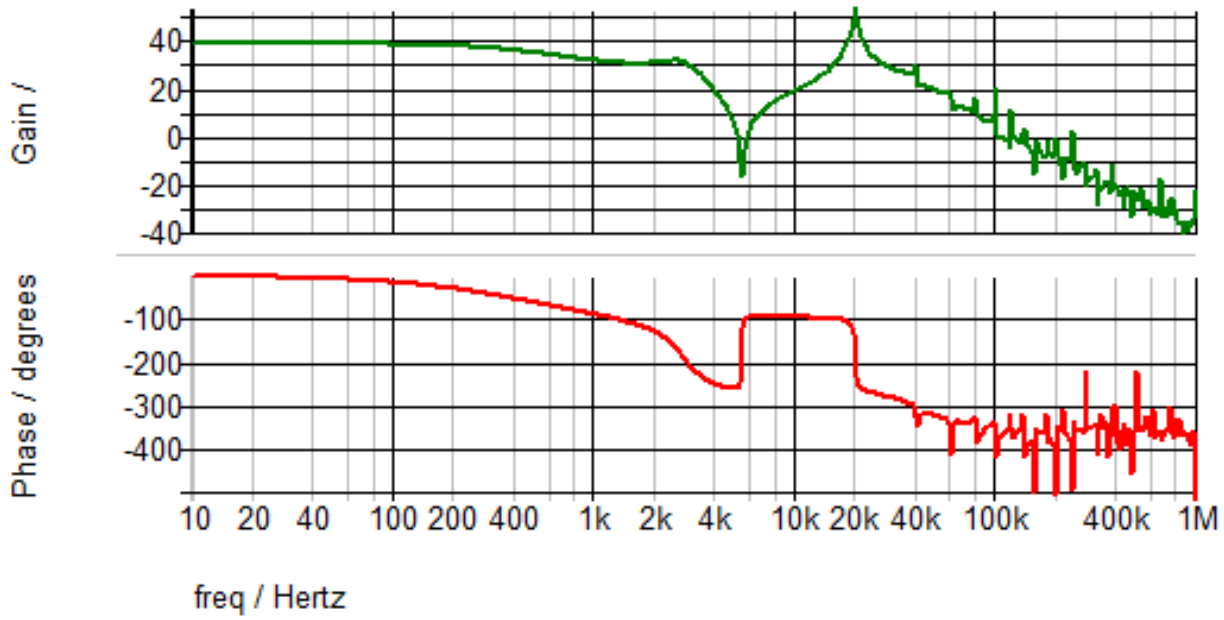

Fig. 4.8: PSIM boost mode simulation results

Once again, the results are imported into sisotool for PI controller design. This system is unique and thus the ideal phase margin, gain margin, and bandwidth is difficult to achieve. Therefore, the ideal parameters are sacrifised and the phase margin is settled to be 31˚, gain margin equal to 10.9 dB, and bandwitch of 465 Hz, as shown in Figure 4.9.

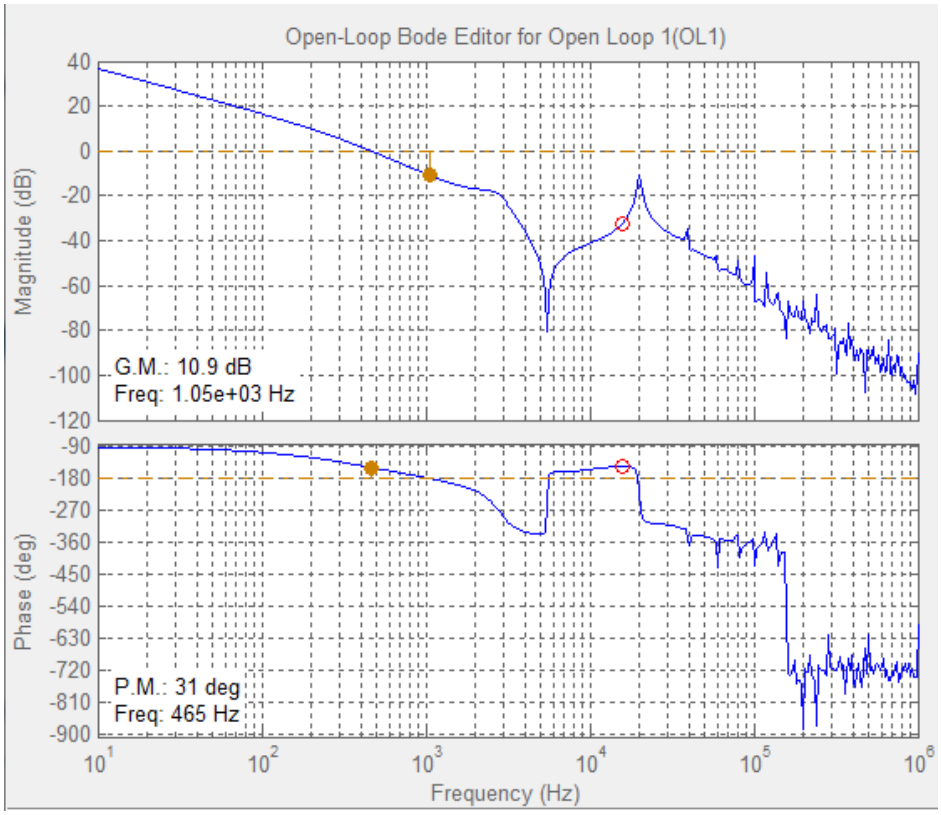

Fig. 4.9: Sisotool for boost mode with controller

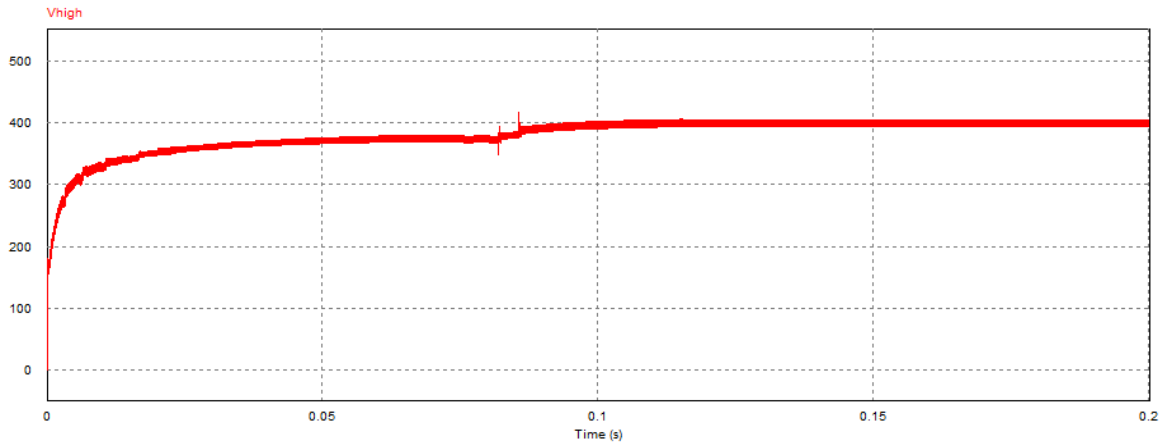

Fig. 4.10: Output voltage in closed loop

Although the system doesn't have the phase margin, gain margin, and bandwidth that is ideal, the system is still stable for operations. Figure 4.10 shows the results of the

output voltage in closed loop. Although the system appears stable,the controller must later be tuned to work in real experimental applications, similar to buck mode operations. The tuning and calibrations will be done with coding of the dsp controller.

4.3 Controller

The actual implementation of the closed loop controller as well as the gating signals shown previously in PSIM is done digitally through the Texas Instruments TMS320F28335 DSP chip. The voltage and current sensor chips are ACPL-C870 and LEM LTSR-15NP respectively. The sensor chips gains are tuned while converting from analog to digital converter (ADC) to communicate with the DSP chip. The gate driver chips are Si8235 for the high side switches (Q5-Q8) for its shoot-through protection. Si8233 chips are used for the low side switches (Qc, Q1-Q4), shoot-through protection is not available for this driver to be compatible with the gating logic designed. The entire implementation is done through coding in the easyDSP software. The coding includes the PI controllers, the gating logic for the switching devices, and the gain of the sensors. Digitally programming the PI controller is a lot easier to tune than its analog equivalent. Therefore, it is preferred to use the DSP board with ADC rather than analog circuits. The sensing circuitry and gating control connection in buck mode is shown in Figure 4.1. Here, the sensing includes the low side voltage and current sensing to fulfill the battery charging characteristics. In boost mode, the system is similar to that of buck mode, however only the voltage sensing is needed for high side voltage.

4.4 Flyback and Main Transformer Design

A main portion of the power stage are the transformers, these are required to properly transform the current and voltage from the high side and the low side of the bridges. The flyback transformer is not used as often as it only operates during the start-

up stage, and in the very beginning of the transitional stage of the boost mode operations. However, the flyback transformer is significant for functioning as an inductor for regular boost mode, buck mode, and most of the transitional stage operations.

4.4.1 Flyback Transformer Design

The flyback transformer is used to transform energy during the start-up of the boost mode. Because this transformer's common use is to function as an inductor, the side of the flyback transformer on the main power path must first be designed as an appropriate inductor.

In order to create an output LC low pass filter for appropriate ripple current during buck mode operations, the output bus capacitor is selected to be 20 µF and the inductor 150 µH. Given ferrite cores, the max flux density ($B_{max)}$ is selected to be 0.2 T, and fraction of core window area (Kµ) of 0.5, and maximum current density (J_{max}) of 150 A/cm^2. With the equation below, core area multiplied by core window area (A_C*W_A) can be calculated:

$$A_C * W_A \geq L1 * \frac{I_{1max} * I_{1rmsmax}}{K_\mu * B_{max} * J_{max}} * (1 + \frac{n_2}{n_1} * \frac{I_{2rmsmax}}{I_{1rmsmax}})$$

From this equation, an appropriate core size (given the availability in the lab) is the EE80 ferrite core. The current through the inductor is at 20.83 A at full load, therefore, an appropriate wire (given availability in the lab) is the gauge 10 round litz wires. On the secondary side of the flyback transformer, the current flow is brief and reaches peak of just 5 A. Therefore, the appropriate wire (given availability in the lab) is the gauge 16 round litz wire. The gauge 10 wire has 8 turns, and the gauge 16 wire has about 70 turns to satisfy the turn ratio of 8.33. The constructed flyback transformer has

magnetizing inductance of 150 µH and leakage inductance of 4 µH. When the flyback transformer is operating as an inductor, the sum of the magnetizing and leakage inductance equates to the inductance of the inductor. Figure 4.11 below shows the results of this flyback transformer attached to a waveform generator [42].

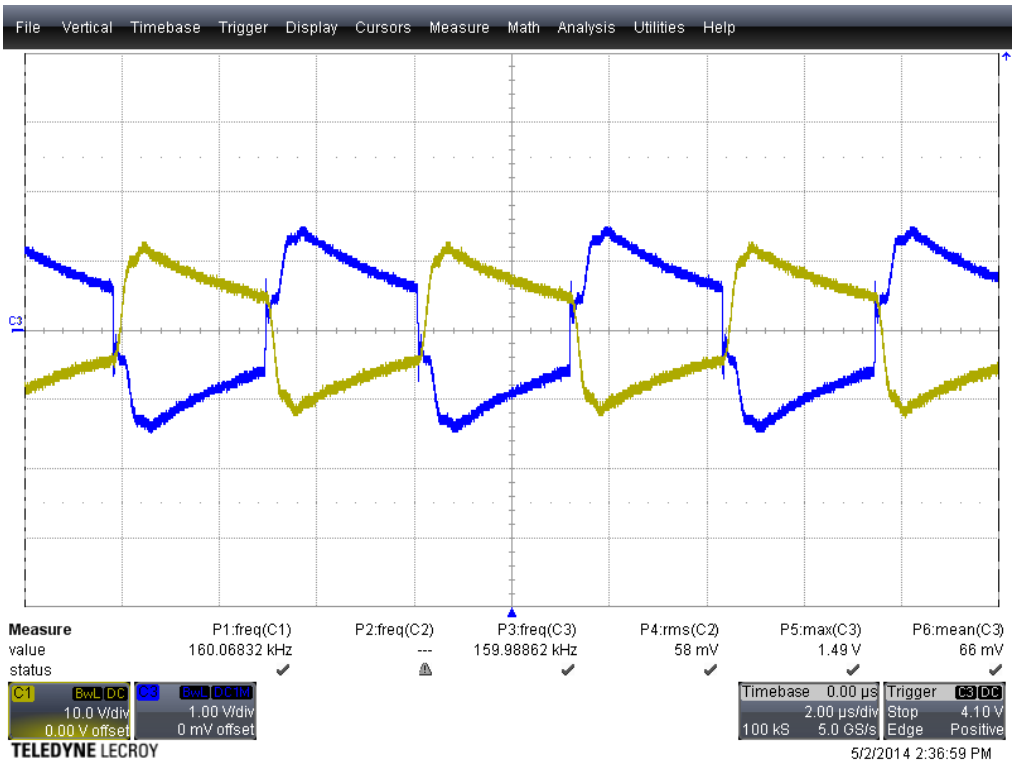

Fig. 4.11: Flyback transformer waveform

As Figure 4.11 shows, the frequency is much higher than the converter's operating frequency of 20 kHz. The high switching frequency is chosen to reduce the voltage spikes generated by the open load. The voltage levels are approximately the same, with the blue curve slightly higher. The yellow curve is 10 V/div whereas the blue is 1 V/div, therefore, the turn ratio is a little less than 10 which is near the goal of 8.33.

4.4.2 Main Transformer Design

The main transformer is responsible for transforming the current and voltage from the low and high sides of the bridges during all stages operations. With the low side nominal voltage of 48 V and high side of 400 V, the current is about 20.83 A at the high current side and about 2.5 A on the low current side. Similar to the flyback transformer design, using ferrite cores, the B_{max} is selected to be 0.2 T, and Kμ of 0.5, and J_{max} of 150 A/cm^2. The duty cycle is selected to be 0.5, Vg is 48 V, switching frequency is 20 kHz, and current is about 21 A. Using the equation below, the appropriate core size can be designed:

$$A_C * W_A \geq \frac{D * V_g * I_{1rmsmax}}{K_\mu * B_{max} * J_{max} * f_s}$$

From this equation, an appropriate core size (given the availability in the lab) is the EE65 core. Given the current parameters above, the high current side needs to handle the same amount of current as the high current side of the flyback transformer. Therefore, the high current side of the transformer is once again using the gauge 10 round litz wire. The low current side has regular current flow, but the current is lower than the low current side of the flyback transformer. The appropriate wire (given availability in the lab) is the gauge 18 round litz wire. The gauge 10 wire has 6 turns, and the gauge 18 wire has 50 turns to satisfy the 8.33 turn ratio. The constructed transformer has the magnetizing inductance of 140 μH and leakage inductance of 2 μH. Figure 4.12 shows the results of this transformer [8].

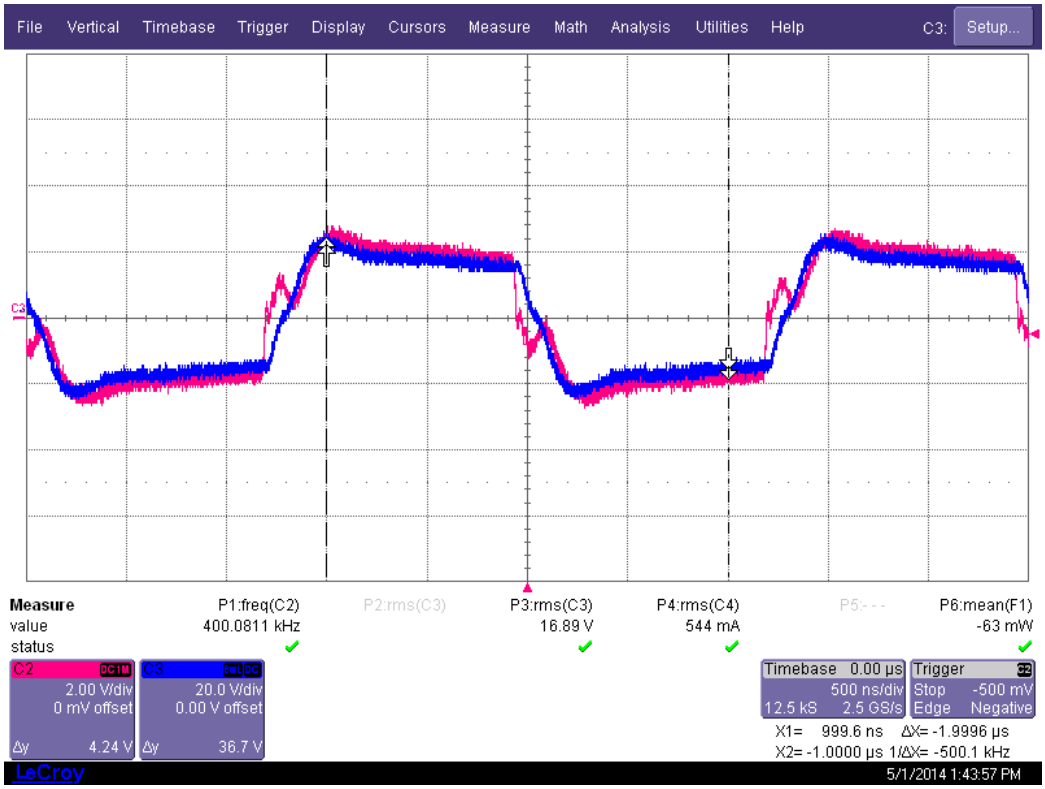

Fig. 4.12: main transformer waveform

As Figure 4.12 illustrates, the frequency is again much higher than the converter's operating frequency to eliminate spikes caused by the open load. The waveforms are nearly identical with the red curve a little larger. The blue curve is 10 times larger per division; therefore, the turns ratio is slightly less than 10 which verifies the functionality of the designed turn ratio as well as the transformer.

CHAPTER 5: Experimental Results

5.1 Buck Mode Experimental Results

The buck mode experimental results for battery charging is difficult to capture on the oscilloscope due to the slow charging and discharging characteristics of a battery or large capacitor. Therefore, the simulation results shown in Figure 4.7 are used to verify the functionality of the battery charging.

5.1.1 Buck Mode Zero Voltage Switching

In order to reduce switching losses, zero voltage switching (ZVS) is preferred for high efficiency. ZVS is confirmed by measuring the gating signal V_{GS} as well as the switch's V_{DS}. ZVS is achieved if V_{DS} falls to zero before V_{GS} turns on the switch. Figure 5.1 shows the schematics of the buck mode operations with the measured switches circled.

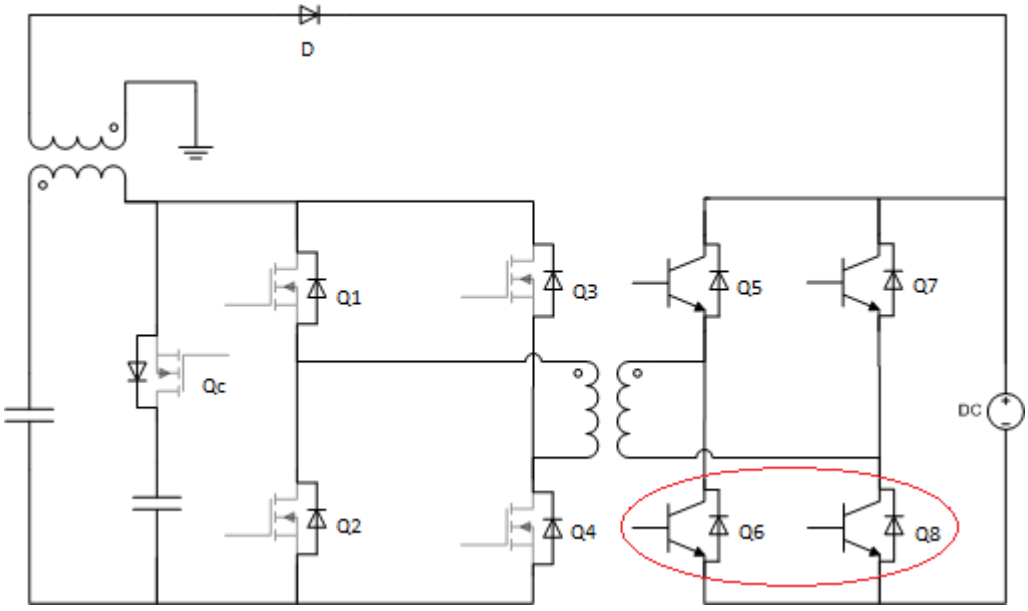

Fig. 5.1: Buck mode schematics with tested switches for ZVS

As Figure 5.1 shows, the bottom switch for both the leading and the lagging legs (Q6 and Q8) are measured. The bottom switches are measured because non-isolated voltage scopes are used for this experiment. Figures 5.2 and 5.3 below show V_{DS} and V_{GS} for the two switches.

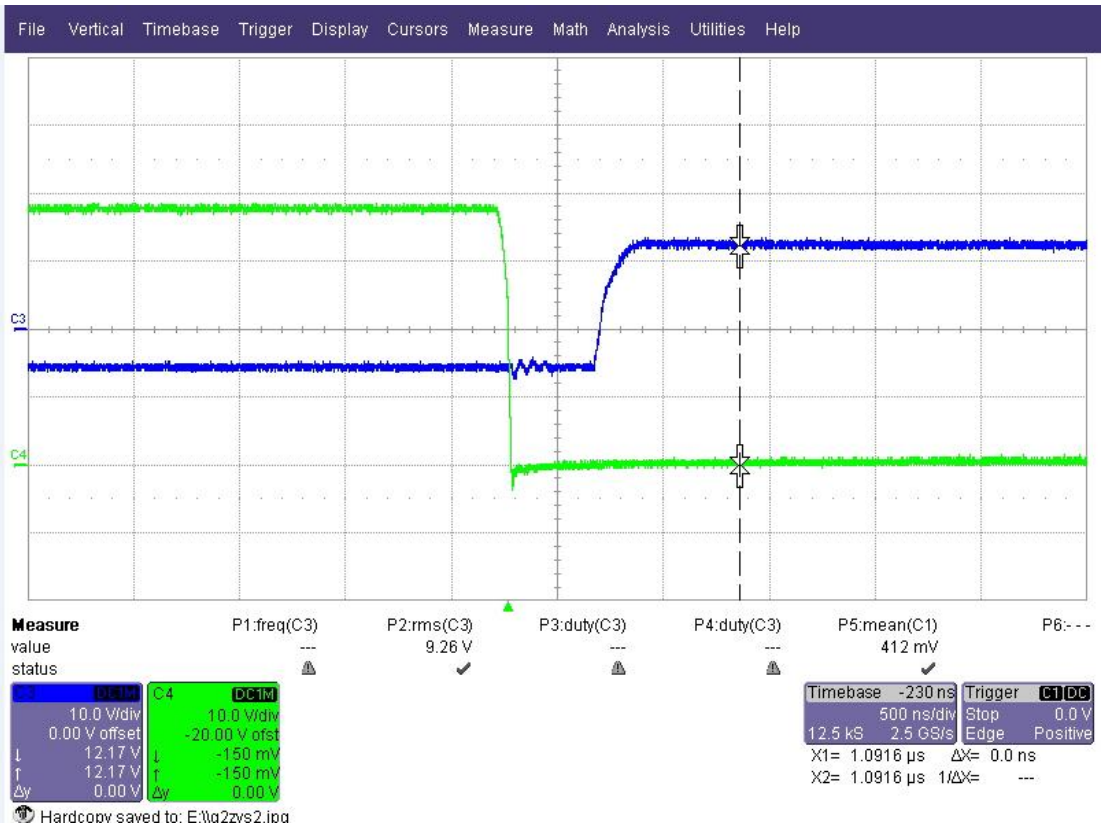

Fig 5.2: V_{DS} and V_{GS} for leading leg bottom switch

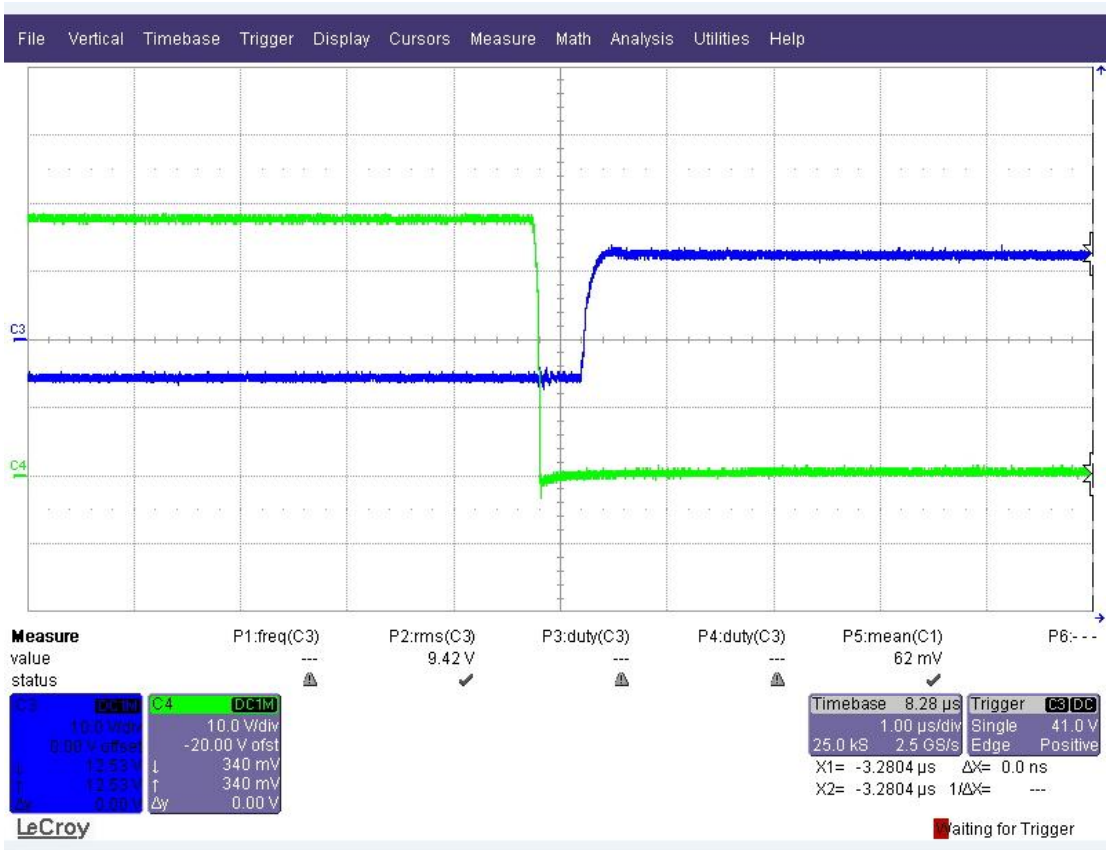

Fig. 5.3: V_{DS} and V_{GS} for lagging leg bottom switch

As the Figures 5.2 and 5.3 show, the V_{DS} (shown in green) reaches 0 before V_{GS} (shown in blue) turns on, therefore, achieving ZVS.

5.1.2 Buck Mode Start-up

To verify that the active clamp also reduces the current spike in buck mode, the transient characteristics are tested. From the simulation results in Figure 4.7, it is concluded that the transient current and voltage spikes are insignificant. Figure 5.4 below shows the experimental results of the transient testing.

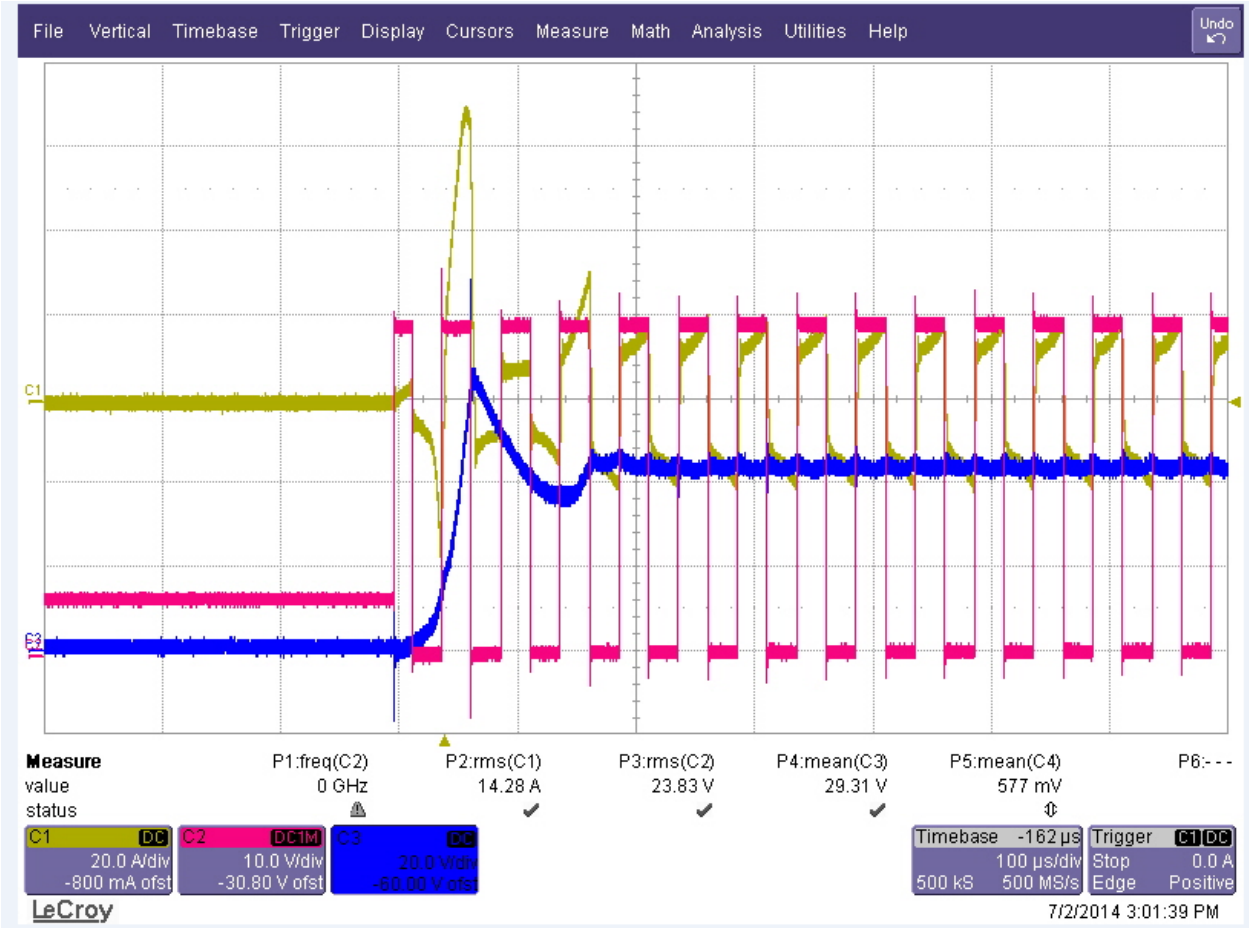

Fig. 5.4: Buck mode transient testing

As Figure 5.4 shows, the current spike (shown in yellow) reaches a peak of about 70 A which is not detrimental to the switches. The voltage spike (shown in blue) is also small and therefore, buck mode is safe for operation. The voltage spike is present because the load used is a resistive load. However, if the output load is a large capacitor or a battery, the voltage spike would be eliminated completely as the voltage would rise slowly as the current is kept constant to charge the battery. The waveforms in Figure 5.4 show that the converter is operational during the transient of the buck mode operations.

5.1.3 Buck Mode Steady State

Figure 5.5 below shows the steady state operation of the converter in buck mode at 100% load.

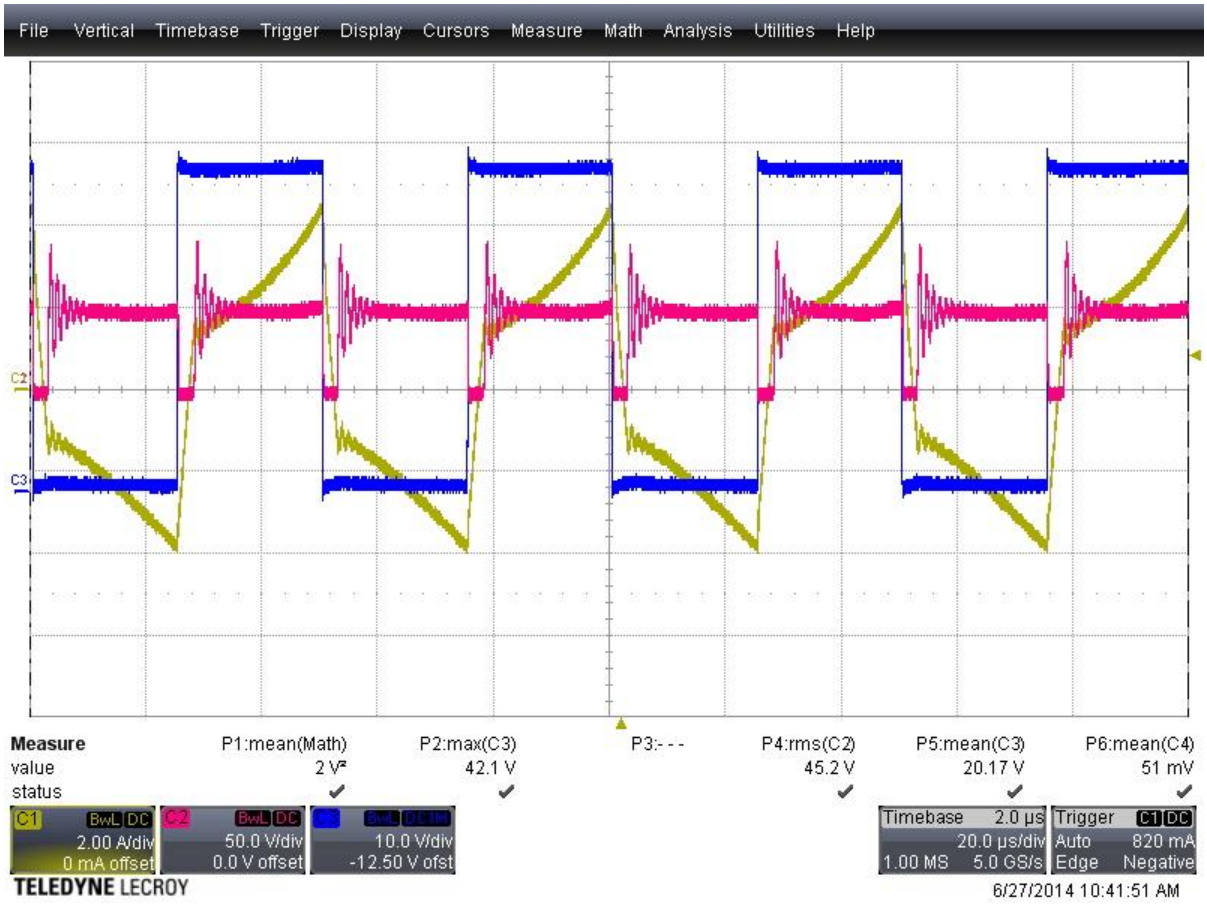

Fig. 5.5: Buck mode steady state testing

As Figure 5.5 shows, the V_{DS} of a main switch (in blue) is shown with the transformer current (in yellow) and the bridge voltage of the low voltage side (in red). The waveforms show a functional converter in buck mode.

With the steady state working with ZVS, the efficiency is measured and shown in Figure 5.6 below.

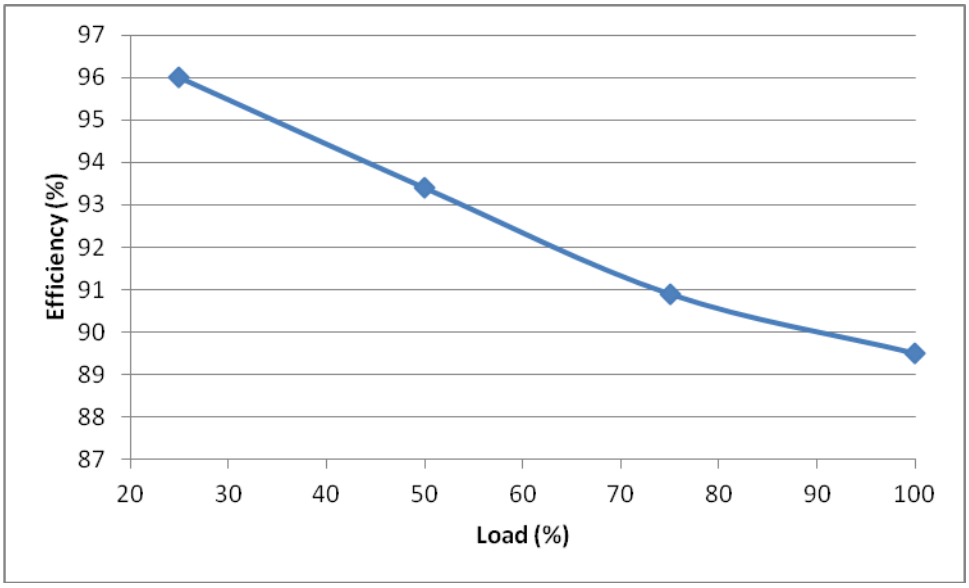

Fig. 5.6: Buck mode efficiency

The majority of the losses lay within the conduction loss because synchronous rectification is not used. The equation of conduction loss for the diodes on the low side is:

$$P_{conduction} = 2 * I * V_{forward}$$

Here, the V_{foward} is the forward voltage drop of the rectifying diodes. Typical V_{foward} of diodes are about 1.2V; however, the voltage drop increases exponentially as the current flowing through it increases. The voltage drop is also lower if the temperature is increased. Therefore, under low load, the V_{foward} is much lower compared to heavier load. This explains why the efficiency of the converter in heavier load is lower than lighter load due to the conduction losses.

5.2 Boost Mode Experimental Results

The boost mode experiments include the start-up as well as for the steady state results. Because the battery is variable between 45 V to 55 V with nominal of 48 V, all three conditions are tested and verified for functionality.

5.2.1 Boost Mode Soft Switching

Similar with the ZVS switching in buck mode, soft switching is also attainable in boost mode. Given the transformer leakages of 2 µH and 4 µH, the proper clamping capacitor is selected to be 70 µF. The calculation for this capacitance can be found in Chapter 4.2. The bridge voltage and current on the low side are analyzed for soft switching. Figure 5.7 shows the schematics of where the scopes are measuring.

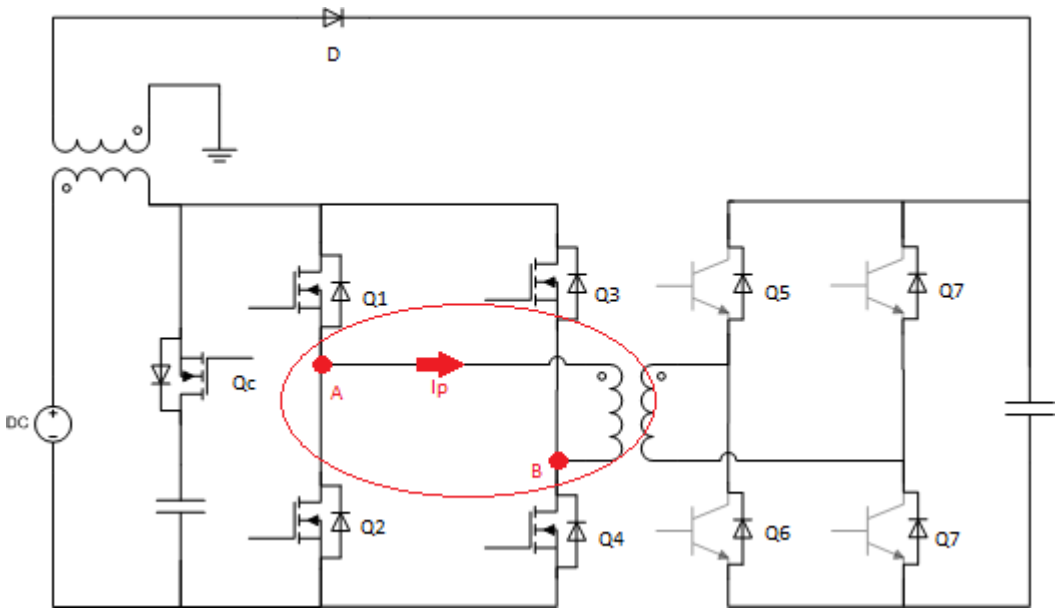

Fig. 5.7: Boost mode soft switching testing schematics

As shown in Figure 5.7, the primary current (I_P) is measured along with the voltage across the points of A and B. Figure 5.8 and 5.9 below show the waveform results of the tested points in Figure 5.7

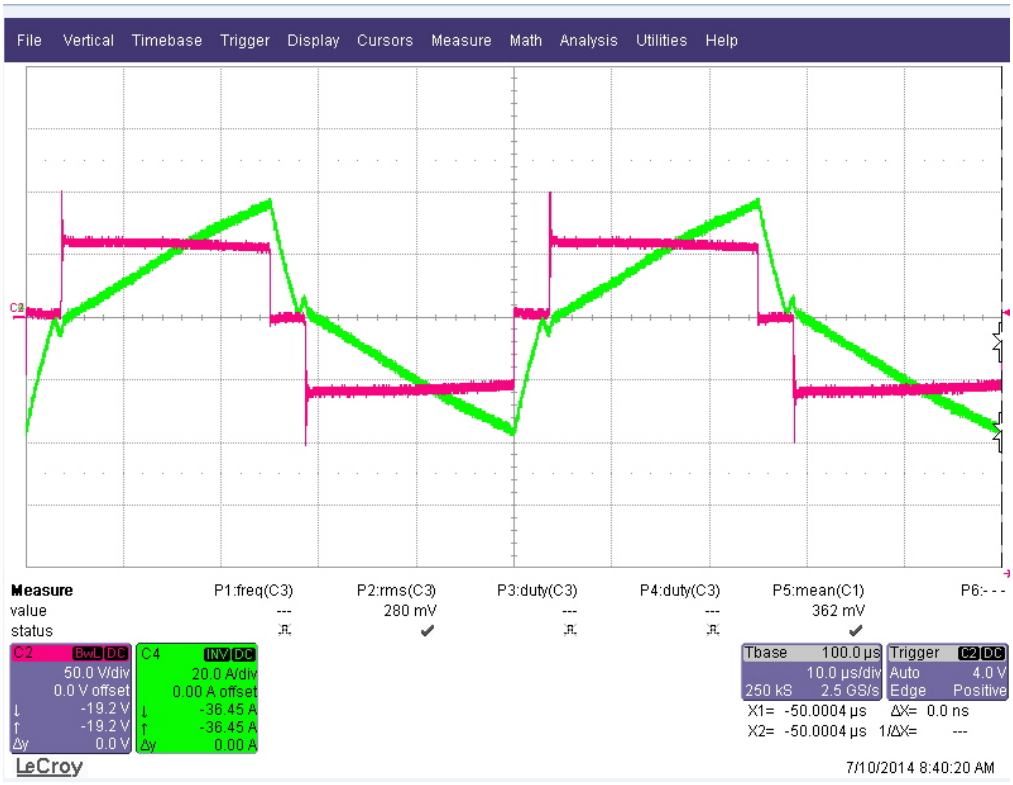

Fig. 5.8: Boost mode bridge voltage vs. current

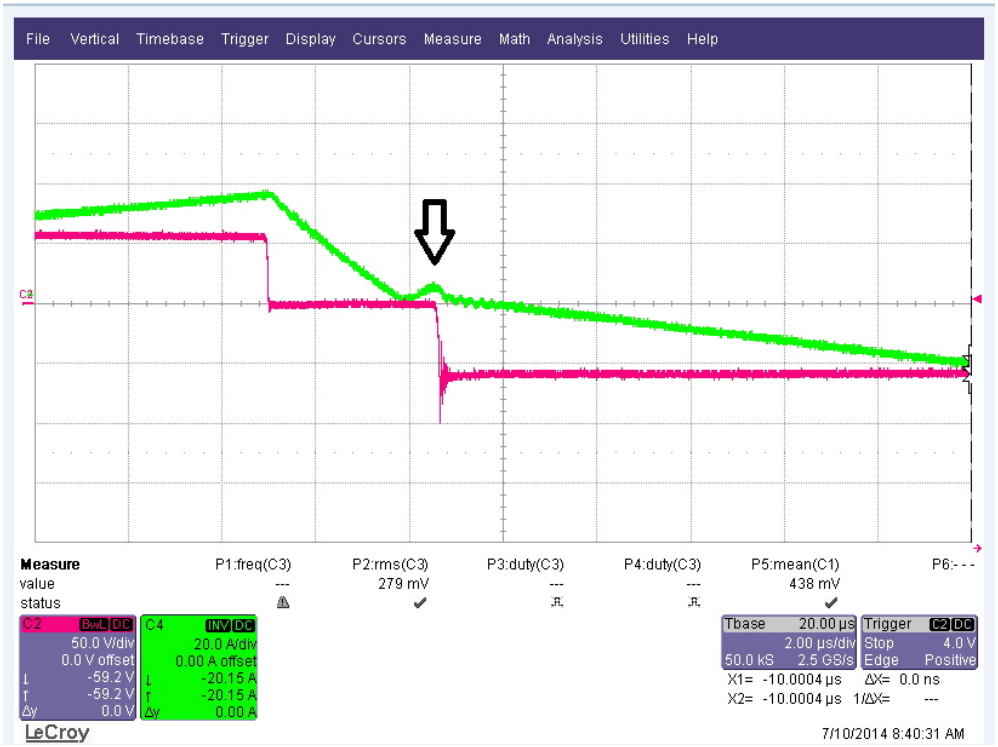

Fig. 5.9: Buck mode bridge voltage vs. current zoomed

In Figures 5.8 and 5.9, the bridge voltage is in red and the bridge current is in green. As these Figures show, when the voltage goes from 0 to high, the current is flowing in the negative direction. This indicates that the circuit is attaining zero current switching (ZCS) for turn-on.

However, the figures acquired are not clear enough to verify ZVS, therefore, the same technique used for buck mode are used for boost mode. Once again the bottom switch of both the leading and lagging legs are measured (Q2 and Q4), the schematics for the circuit tested are shown below in Figure 5.10.

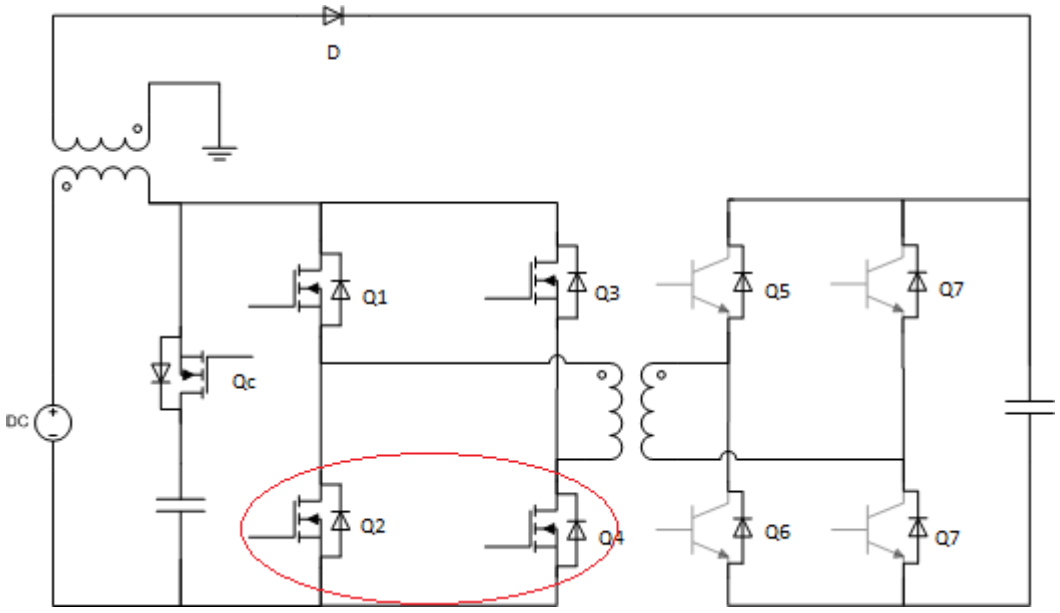

Fig. 5.10: Boost mode schematics with tested switches for ZVS

Figures 5.11 and 5.12 below show the V_{DS} and V_{GS} for the tested switches to verify ZVS switching.

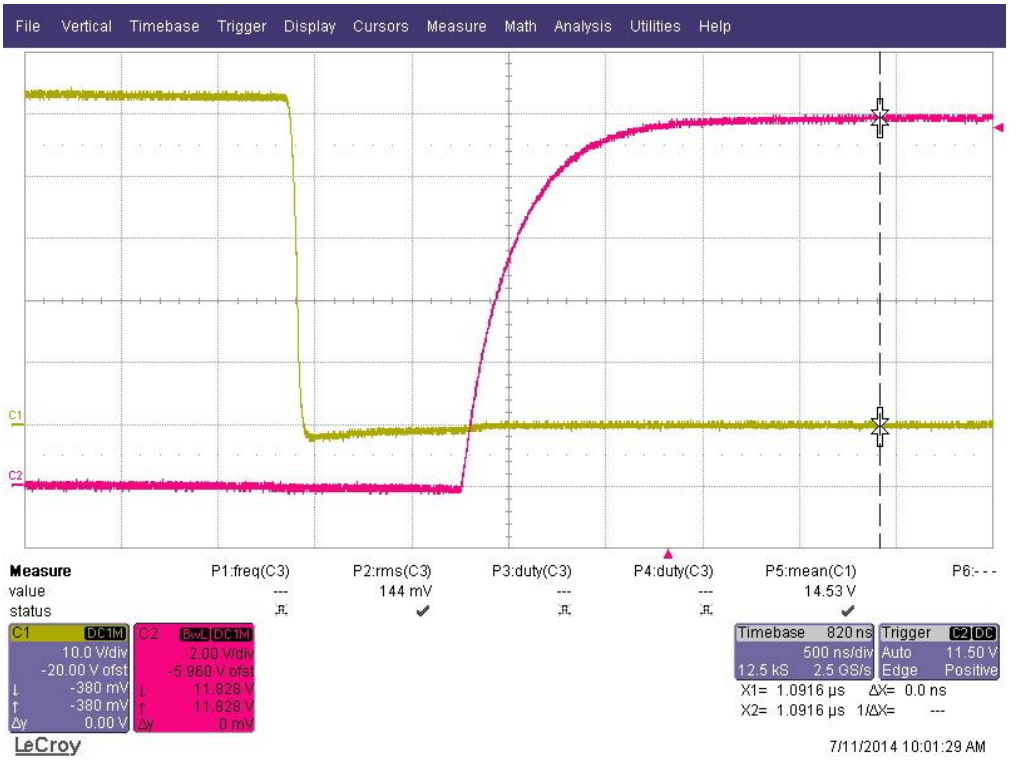

Fig. 5.11: V_{DS} and V_{GS} for leading leg bottom switch

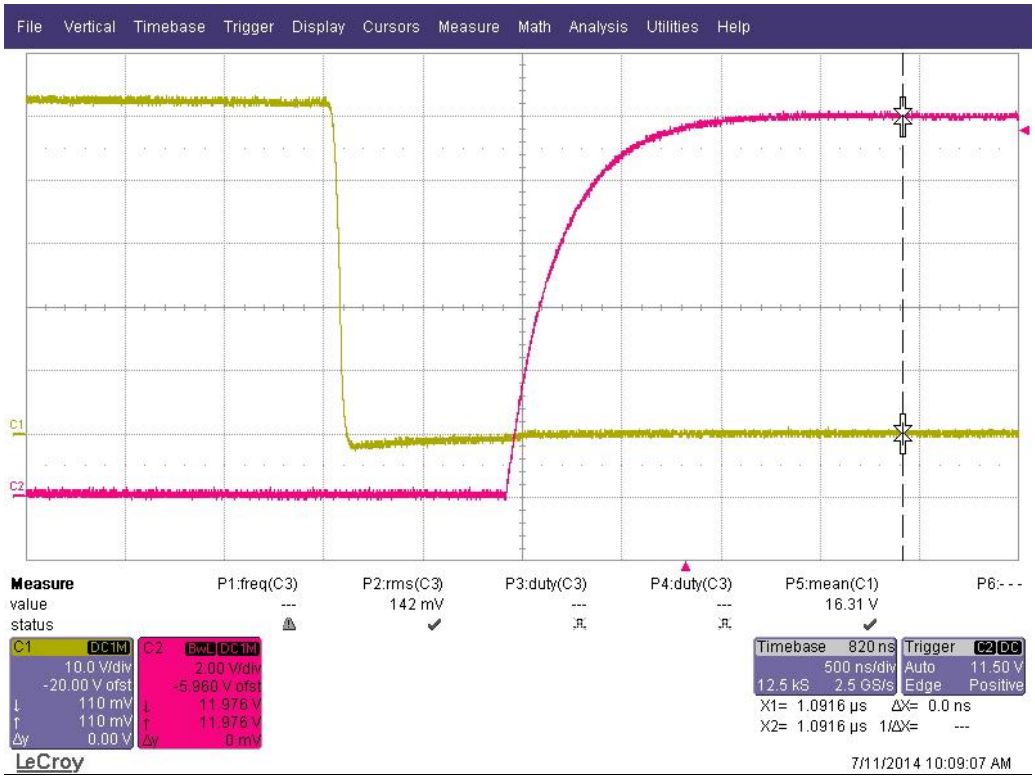

Fig. 5.12: V_{DS} and V_{GS} for lagging leg bottom switch

As Figures 5.11 and 5.12 show, the V_{DS} of the switches reaches 0 before the V_{GS} of the devices turn on, verifying that ZVS is achieved. With these figures, it can be concluded that the converter is operating with soft switching achieving ZVS and ZCS turn on.

5.2.2 Boost Mode Start-up

As discussed, the start-up is a huge problem for the full-bridge converter in boost mode. The transitional stage to eliminate the current spike proposed in Chapter 3 is tested for functionality.

As Figure 3.5 suggests, the clamping switch and capacitor have a voltage stress of 150V across it when the duty cycle reaches 0.5. Although achievable, the switches and capacitor selected (with availability) are rated for 100 V. Therefore, additional implementations must be included for the transitional stage to be operational with the components selected. Because the voltage stress increases as the duty cycle approaches 0.5 during start-up mode (where the duty cycle of the clamping switch is approaching 0), lower duty cycle corresponds to lower voltage stress. When the duty cycle reaches 0.35, the voltage stress across the clamping switch is just under 100 V; therefore, a small jump is made for the converter to go into the transitional stage when the duty cycle reaches 0.35 instead of 0.5. Because the jump of duty cycle is not significant, the original result in Figure 3.3 (duty waveforms of switches) is not altered considerably. Figure 5.13 and 5.14 below show the simulations of the duty cycle, the transformer current, the output voltage, and the voltage stress of the clamping switch for the converter in boost mode.

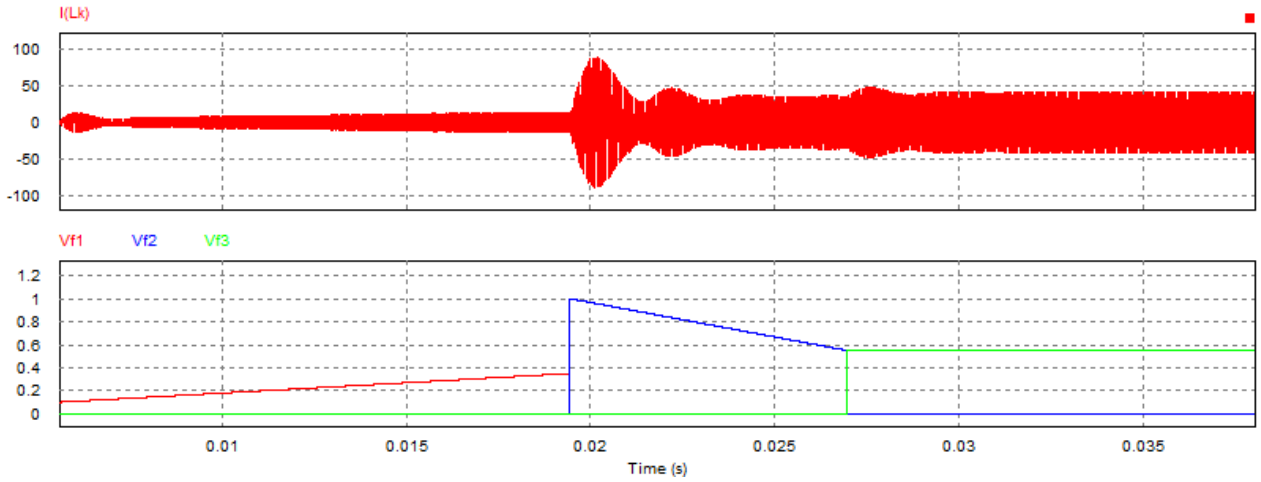

Fig. 5.13: Transformer current vs. duty cycle of used start-up

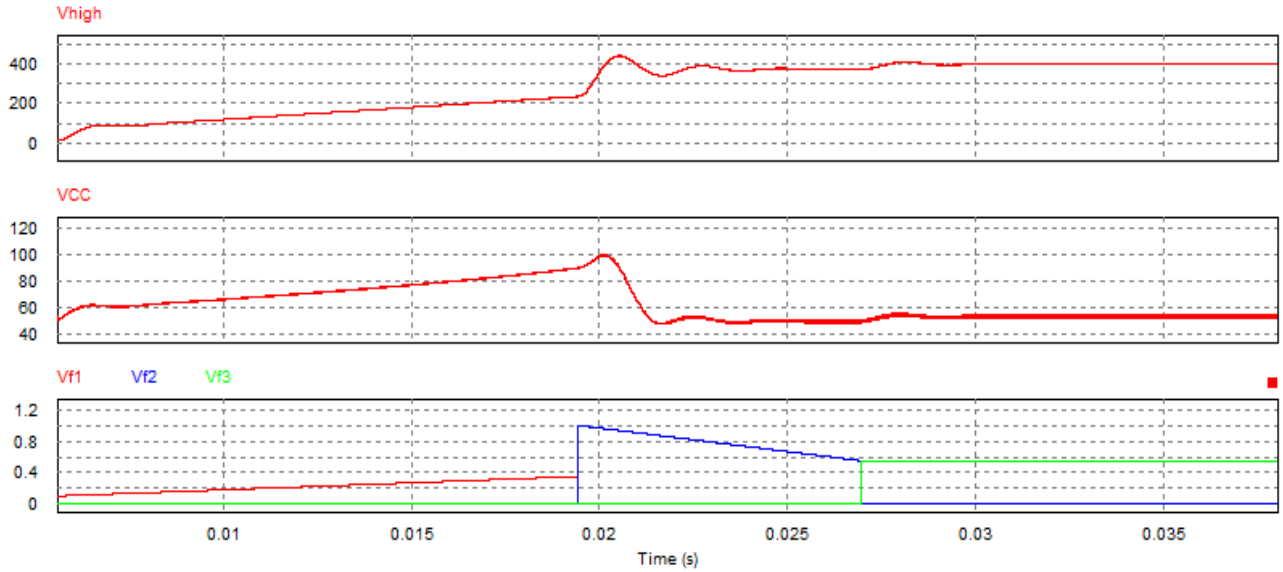

Fig. 5.14: Output voltage vs. voltage stress vs. duty cycle of used start-up

As shown in Figures 5.13 and 5.14, the transitional stage occurs when the duty cycle in the start-up reaches 0.35 instead of 0.5. The transformer current spike is actually reduced slightly as compared to when the transitional stage occurred at 0.5 duty cycle. This is because when the transitional switch occurs, the voltage stress of the clamping switch is lower meaning there isn't as much voltage across the clamping capacitor when the transitional stage occurs. However, the amount of current spike reduction is

insignificant. Having the converter enter transitional stage sooner causes higher voltage spike as the duty cycle jump creates a very fast voltage change. Therefore, it is not necessarily better to have the transitional stage occur earlier. Since the voltage stress is reduced significantly, the selected components can be used for experimentations.

Figure 5.15 below shows the experimental results of the converter during the start-up, transitional, and boost stages with 48 V input.

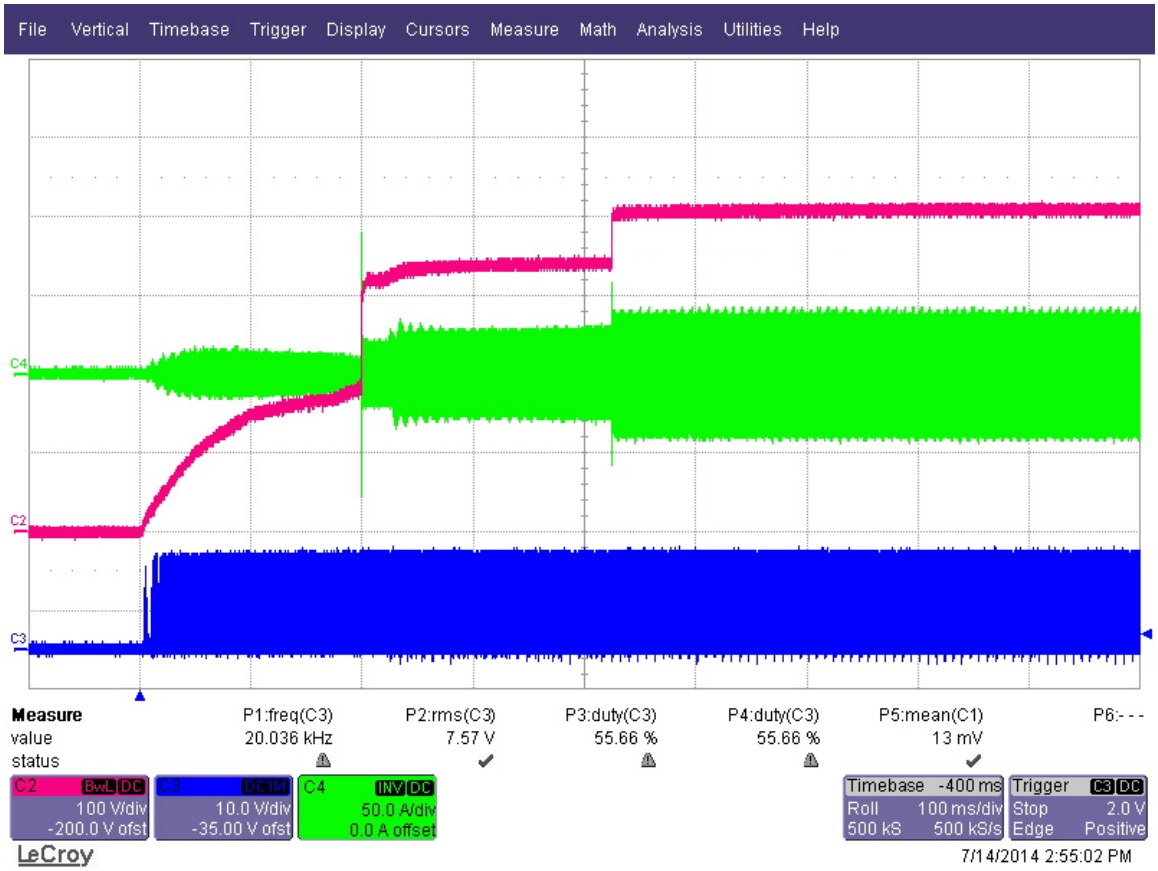

Fig. 5.15: Start-up testing for 48 V input

In Figure 5.15, the gating signals (blue) is used to trigger the scope for capturing, the output voltage (red) transitions from start-up mode to transitional stage then to regular boost mode. The current of the transformer (green) peaks at about 80 A as predicted from the simulation results.

Figure 5.16 and 5.17 shows the same start-up testing for 45 V and 55 V input respectively.

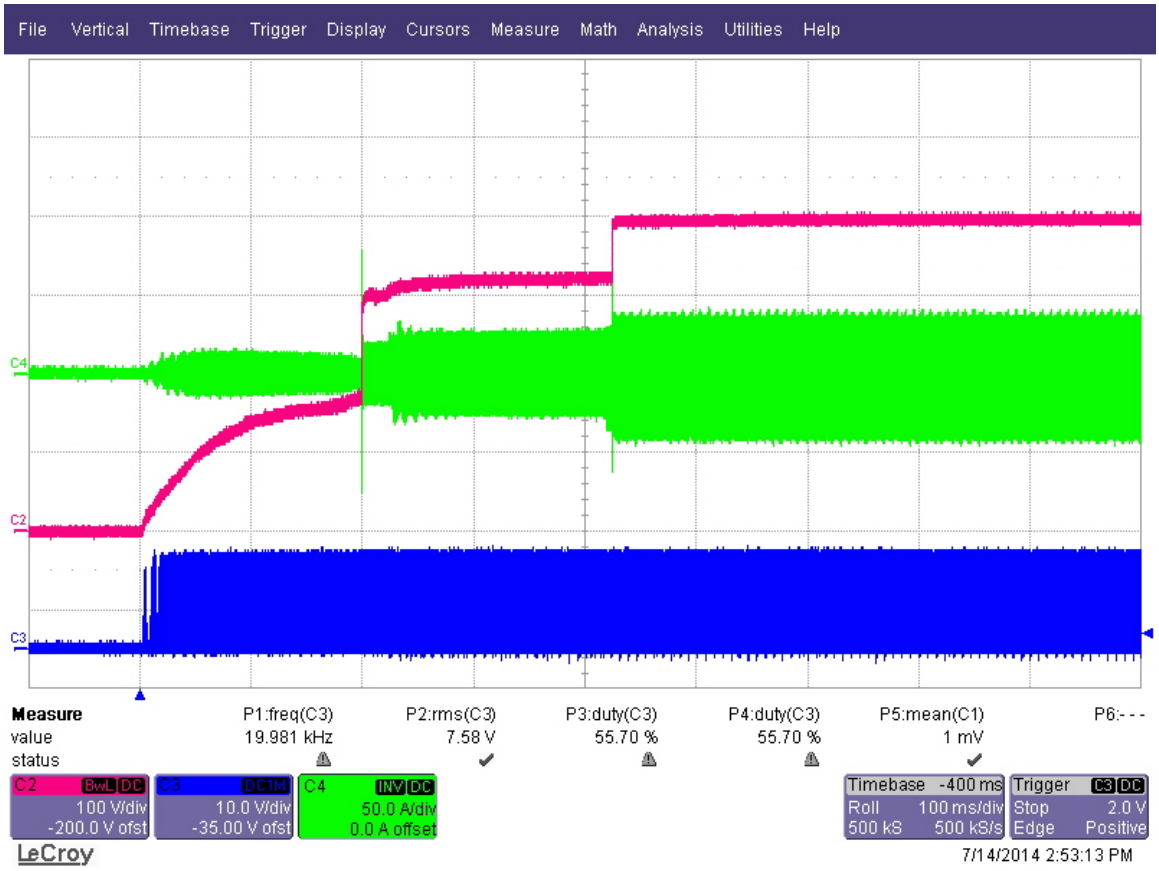

Fig. 5.16: Start-up testing for 45 V input

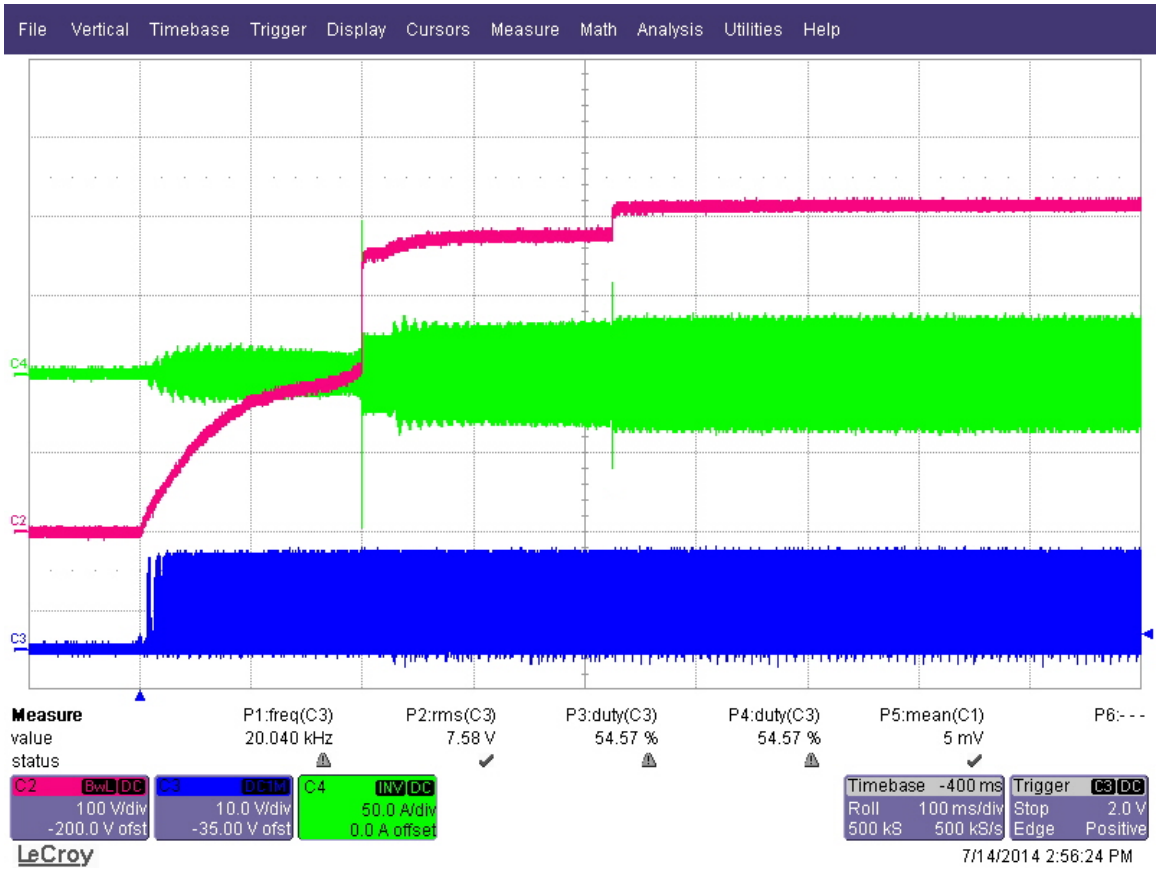

Fig. 5.17: Start-up testing for 55 V input

As suggested in Figures 5.14 through 5.16, the current spike is under 100 A even at the worst case of 55 V input. These experimental results show that by including the transitional stage, it is much safer for the converter to transition from start-up mode to boost mode as the current spike is significantly reduced. At nominal input voltage, the current spike is reduced from the simulated 400 A (this result could not be verified as the switching devices are destroyed in the process) to about 80 A, which is a considerably lower current level for devices.

5.2.3 Boost Mode Steady State

The steady state waveforms are shown below in Figure 5.18; here, the bridge voltage (before the active switches), V_{DS} for an arbitrary switch, and the transformer current are shown.

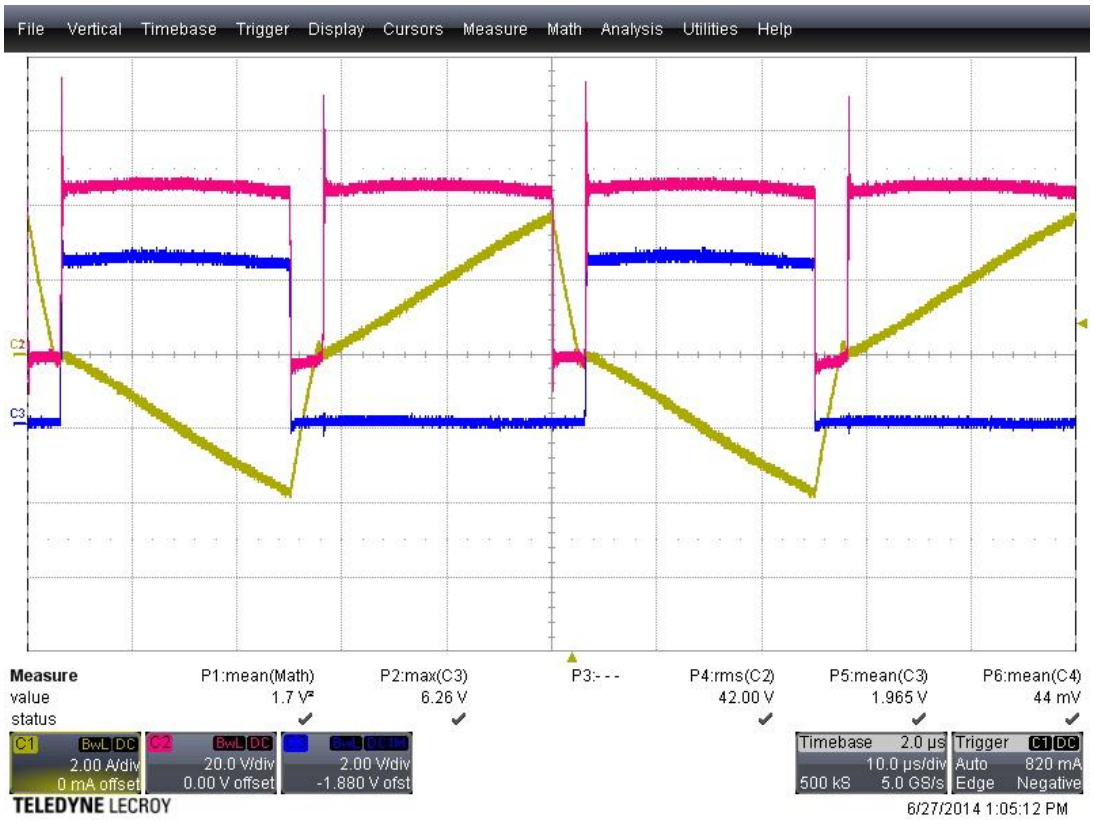

Fig. 5.18: Boost mode bridge voltage vs. transformer current vs. V_{DS}

In Figure 5.18, the bridge voltage is in red, V_{DS} is in blue, and the transformer current is in yellow. Figure 5.19 shows the efficiency of this converter in boost mode during steady state.

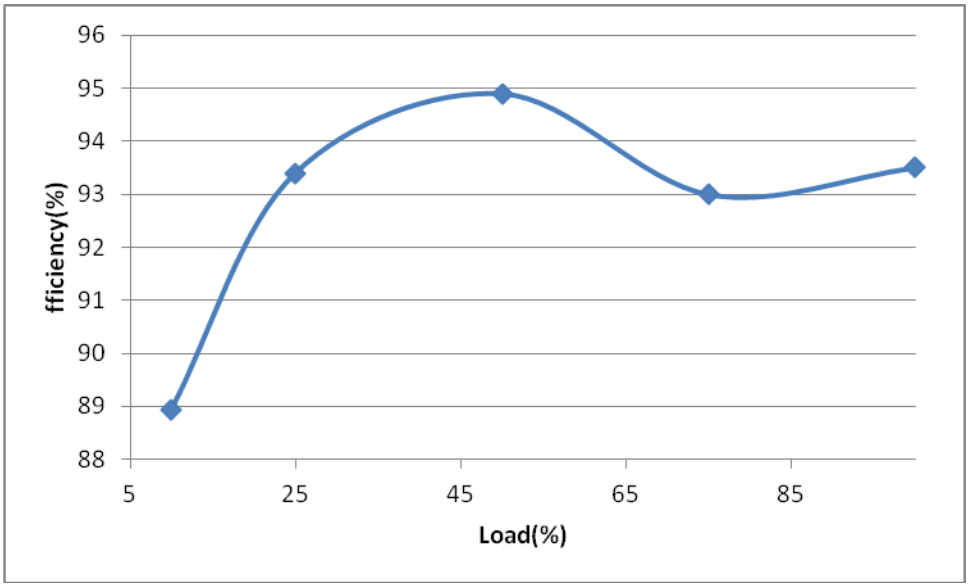

Fig. 5.19: Boost mode efficiency

As Figure 5.19 shows, the efficiency is generally higher with higher load. This is opposite of the buck mode operation because the conduction losses from the rectifying diodes are significantly smaller with the lower current on the high voltage side. Therefore, there is not significant of losses due to conduction at full load. However, extra switching losses are introducted by the extra clamping switch which is not present during buck mode operations.

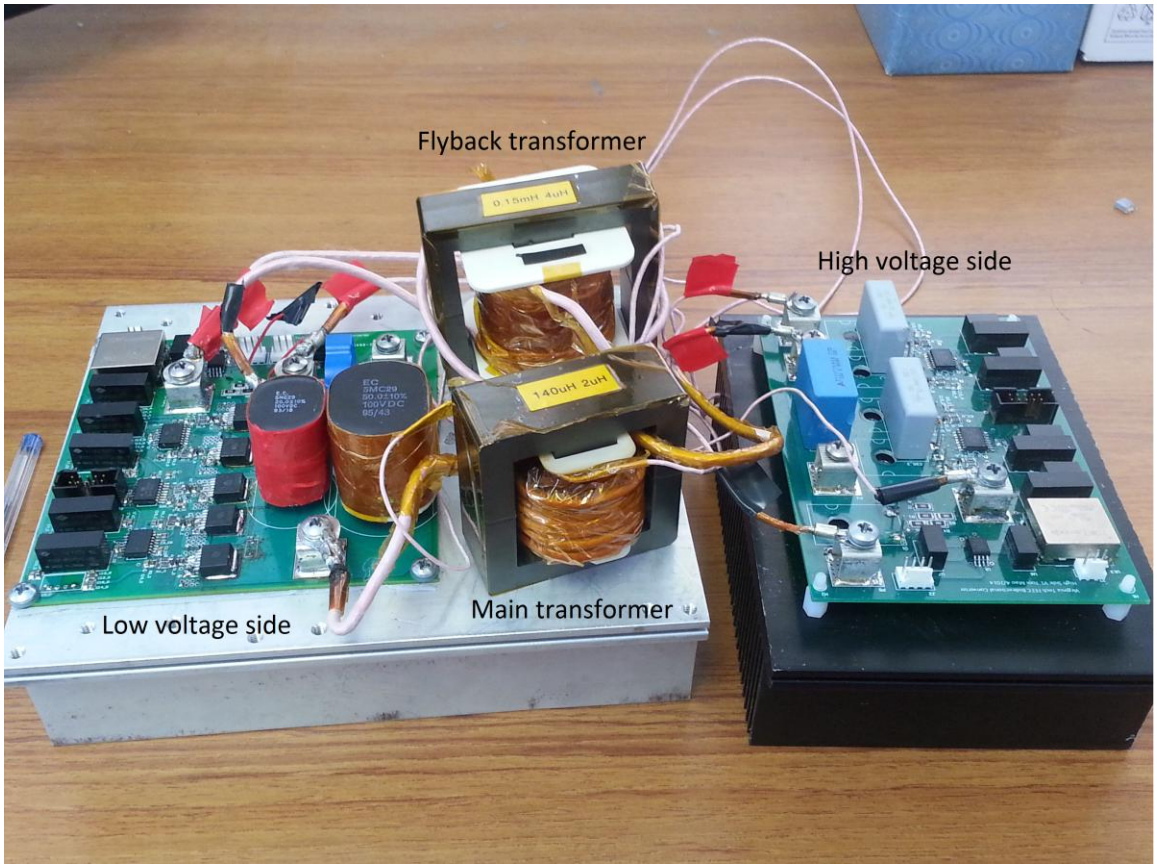

Fig. 5.20 Constructed bi-directional dc/dc converter

The overall converter is shown in Figure 5.20. Both the high side and the low side printed circuit board (PCB) is less than 25 inches^2 in area.

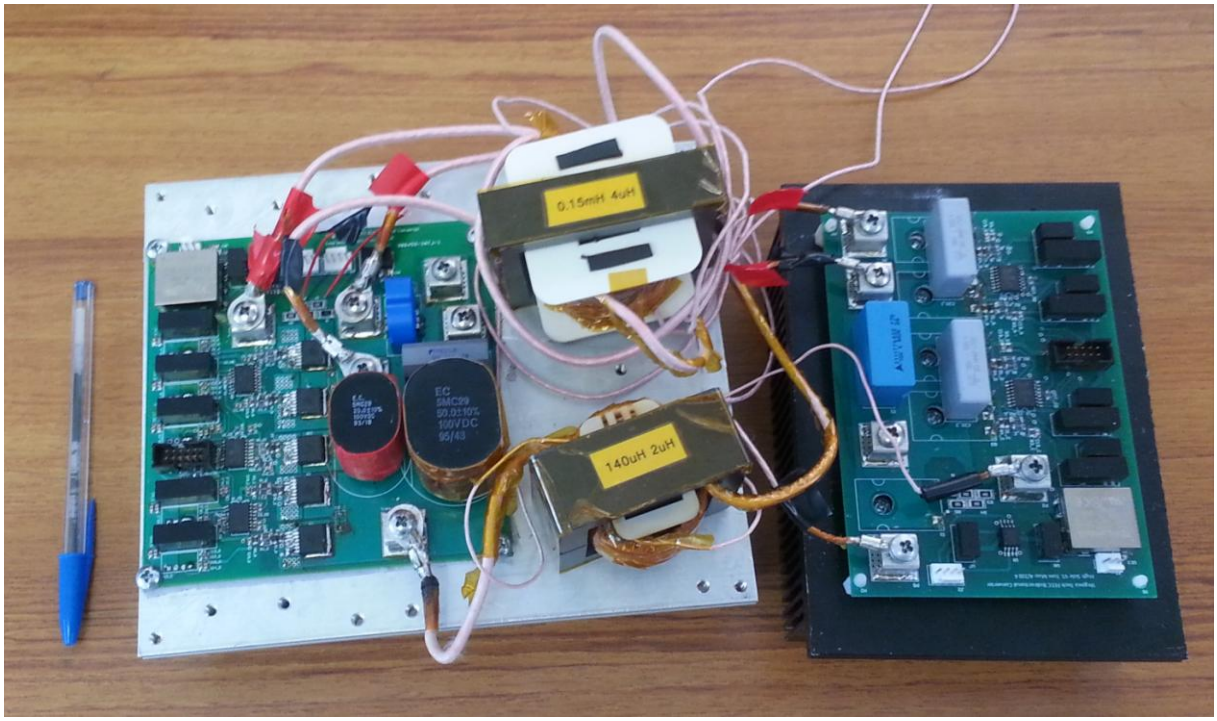

Fig. 5.21: Constructed bi-directional dc/dc converter in top view

Figure 5.21 shows the top view of the constructed bi-directional dc/dc converter with a pen for comparison. As the Figure suggests, the complete converter does not take a lot of space. The low voltage side board is a 4 layer PCB board and its area is larger than the high voltage side board's as it needs more copper area to handle the high current. Similarly, the transformer winding wires are thicker on the low voltage side for the same purpose of current handling.

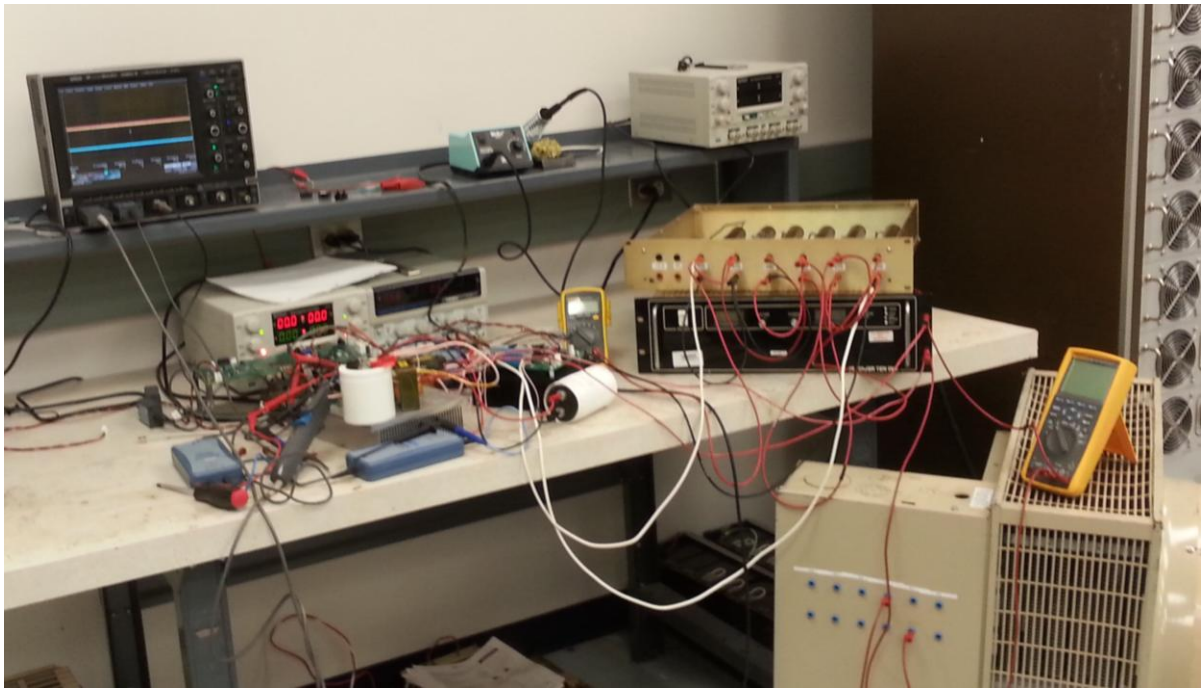

Fig. 5.22: Test setup of bi-directional dc/dc converter

Figure 5.22 shows the overall setup during experimental testing of the bi-directional converter. As the Figure suggests, oscilloscopes, power supplies, DSP board, and multimeters are used to test and capture the functionality of this isolated bi-directional dc/dc converter. The following table shows the components used for this project.

Component Name	Part Number
Qs, Q1-Q4	IPB025N10N3
Q5-Q8	IKW40N65F5
D	APT30DQ100
Cc	Electronic Concept 5MC29 (50µF, 20µF)

CHAPTER 6: Conclusion

In conclusion, an isolated bi-directional dc/dc converter using the full-bridge with active clamp topology and smooth transitioning is designed and tested in this thesis. The bi-directional dc/dc converter is very commonly used for its usefulness in battery charging and discharging. The start-up in boost mode has always been a problem for full-bridge topology. However, the full-bridge topology is very useful for high power applications and, thus, the start-up problem must be solved. Although a start-up solution was proposed before, the transition from start-up to boost mode still presents a problem with a large current spike from the fast discharge of the clamping capacitor. The proposed transitional stage does not change the topology or the previous start-up and boost stage. Instead, a transitional stage is included that requires nothing more but extra gating logic which is be done very easily with the DSP board. This transitional stage significantly reduces the current spike caused by the fast discharge of the clamping capacitor by having a more gradual discharge while not interrupting the main power path flow. Moreover, the transitional stage does not affect the steady state operations of the originally designed bi-directional dc/dc converter.

6.1 Future Work

Although successful, there are some potential future work that can improve the overall converter performance. The first suggestion for future work is to introduce synchronous rectification to reduce conduction losses of the rectifying diode bridge. Reducing the conduction losses will significantly increase the buck mode efficiency during higher loads.

Another action to improve the design is to change the packaging of the low voltage switches (Qc, Q1-Q4). For availability, TO-263-7 MOSFETs are used. These MOSFETs are surface mount devices, therefore, extra copper area as well as a unique heat sink attachment is introduced. The footprint (on the top layer) is connected to the heat sink (clamped to the bottom of the board) with via-pads and thermal pads. Because of the different heat sink attachment, the heat sink capability isn't nominal. Instead, TO-220 or TO-247 through-hole packaging can be used as their main device area can be attached directly to the heat sink. The clamping of the device area to the heat sink can improve the heat transferring of the MOSFETs. TO-247 and TO-220 also have a larger area, which means they allow more current. There are also have more types of MOSETs available in either of these packages than in the TO-263-7 package.

The last suggestion for improvements to the design is to redesign the main transformer core to be more suitable for the developed prototype (48 V - 400 V). When observing the converter through the thermal camera in buck mode, the items with the highest temperature are the low voltage side switches (due to conduction losses) and the main transformer core. This suggests that the transformer could be designed better for the operating parameters. Redesigning the transformer was not an option due to time restraints, but a better transformer can reduce core and winding losses and improve the overall converter efficiency. Although still fully functional, these future work can significantly improve the overall converter performance.

References:

[1] S. Huang, B. S. Hodge, S.F. Pekny, G. V. Reklaitis, "The Value of Battery Storage and Discharge Logic with Solar Microgeneration", *20th Century Symposium on Computer Aided Process Engineering -ESCAPE20*, 2010

[2] S. Janjornmanit, S. Panta, "Novel Battery Charging and Discharging Control System for Solar Panel using One-by-one Controllers and Maximum Power Point Tracker", *Electrical Engineering/Electronics Computer Telecommunications and Information Technology (ECTI-CON)*, pp.78-82, 2010

[3] L. Tao, L. Mo, S. Liu, R. X. Gao, "Optimal Battery Charge and Discharge Control Scheme under Solar Power Inflow", *Instrumentation and Measurement Technology COnference (I2MTC)*, pp. 849-854, 2012

[4] R. Redl, "Batteries for Beginners", *Proc. APEC, Feb.5-9*, 2012

[5] C. Blake, C. Bull, "IGBT or MOSFET: Choose Wisely", Available: http://www.irf.com/technical-info/whitepaper/choosewisely.pdf

[6] H. Li, F. Z. Peng, J.S. Lawler, "A Natural ZVS Medium-Power Bidirectional DC-DC Converter with Minimum Number of Devices", *Industry Applications, IEEE Transactions on Volume: 39*, pp. 525-535, 2003

[7] M. Jain, M. Daniele, P.K. Jain , "A Bidirectional DC-DC Converter Topology for Low Power Application", *Power ELectronics, iEEE Transactions on Volume 15*, pp. 595-606, 2000

[8] D. Zu, C. Zhao, H. Fan, "A PWM Plus Phase-Shift Control Bidirectional DC-DC Converter", *Applied Power Electronics Conference and Exposition, APEC '03*, pp. 641 - 647, 2003

[9] H. Fan, H. Li , "High Frequency High Efficiency Bidirectional DC-DC Converter Module Design for 10kVA Solid State Transformer", *Applied Power Electronics Conference and Exposition, APEC 2010*, pp. 210-215, 2010

[10] L. Wang, Z. Wang, H. Li, "Asymmetrical Duty Cycle Control and Decoupled Power Flow Design of a Three-port Bidirectional DC-DC Converter for Fuel Cell Vehicle Application", *Power Electronics, IEEE Transactions Volume 2*, pp. 891-904, 2012

[11] W. Choi, J. Ju, S. Park, K. Kim, Y. Lim, "Zero-Current Soft-Switching Bidirectional DC-DC Converter for High Efficiency DC Uninterruptible Power Supply", *Telecommunications Energy Conference*, pp. 1-3, 2009

[12] L. Yang, T. Liang, "Analysis and Implementation of a Novel Bidirectional DC-DC Converter", *Industrial Electronics, IEEE Transactions on Volume 59*, pp. 422-434, 2012

[13] S. Inoue, H. Akagi, "A Bidirectional DC-DC Converter for an Energy Storage System with Galvanic Isolation", *Power Electronics IEEE Transactions on Volume 22*, pp. 2299-2306, 2007

[14] K. Wang, L. Zhu, D. Qu, H. Odendaal, J. Lai, F. C. Lee, "Design, Implementation, and Experimental Results of Bi-directional Full-bridge DC/DC Converter with unified Soft-switching Scheme and Soft-starting Capability", *Power Electronics Specialists Conference, IEEE 31st Annual*, pp. 1058-1063, 2000

[15] "Design of Switch Mode Power Supplies", Jan. 2006, Available: http://schmidt-walter.eit.h-da.de/smps_e/smps_e.html

[16] T. Hirose, H. Matsuo, "A Consideration of Bidirectional Superposed Dual Active Bridge DC-DC Converter", *Power Electronics for Distributed Generation Systems*, pp. 39-46, 2010

[17] K. Iida, H. Matsuo, T. Hirose, Y. Ishizuka, "A Novel Bidirectional DC-DC Converter with High Efficiency and Small Size AC Link", *Telecommunications Energy Conference*, pp. 1-8, 2009

[18] T. Hirose, T. Kimura, K. Harada, H. Matsuo, "An Analysis of Bidirectional Superposed Dual Active Bridge DC-DC Converter with Synchronous Rectifier", *TENCON 2010 IEEE Region 10 Conference*, pp. 1241-1246, 2010

[19] F. Krismer, J. Biela, J.W. Kolar, "A Comparative Evaluation of Isolated Bi-directional DC/DC Converters with Wide Input and Output Voltage Range", *Industry Applications Conference*, pp. 599-606, 2005

[20] C. Lin, L. Yang, G. Wu, "Analysis of a Bidirectional DC-DC Converter with Wide Voltage Conversion Range", *Computer, Consumer and Control (IS3C)*, pp. 749-752, 2012

[21] J. Everts, J. Van den Keybus, F. Krismer, J. Driesen, J. W. Kolar, "Switching Control Strategy for Full ZVS Soft-Switching Operation of a Dual Active Bridge AC/DC Converter", *Applied Power Electronics Conference and Exposition (APEC)*, pp. 1048-1055, 2012

[22] Z. Wang, H. Li, "An Integrated Three-port Bidirectional DC-DC Converter for PV Application on a DC Distribution System", *Power Electronics, IEEE Transactions*, pp. 4612-4624, 2012

[23] X. Yan, A. Seckold, D. Patterson, "Development of a Zero-Voltage-Transition Bidirectional DC-DC Converter for a Brushless DC Machine EV Propulsion System", *Power Electronics Specialists Conference*, pp. 1661-1666, 2002

[24] P. Nandankar, M. V. Aware, "High Efficiency Discontinuous Mode Interleaved Multiphase Bidirectional dc-dc Converter", *Power Electronics, Drives and Energy Systems (PEDES)*, pp. 1-6, 2012

[25] W. Chen, S. Wang, X. Hong, Z. Lu, S. Ye, "Fully Soft-Switched Bidirectional Resonant DC-DC Converter with a New CLLC Tank", *Applied Power Electronics Conference and Exposition (APEC)*, pp. 1238-1242, 2010

[26] W. Chen, P. Rong, Z. Lu, "Snubberless Bidirectional DC-DC Converter with New CLLC Resonant Tank Featuring Minimized Switching Loss", *Industrial Electronics IEEE Transactions*, pp. 3075-3086, 2010

[27] M. Suetomi, D. Imamichi, S. Matsumoyo, D. Ueda, J. Yang, Y. Ishizuka, W. Lin, H. Matsuo, "A Novel Bidirectional DC-DC Converter with High Power Efficiency for Isolation in High Voltage DC Power Feeding Systems", *Telecommunications Energy Conference (INTELEC)*, pp. 1-4, 2011

[28] K. Lindberg-Poulsen, Z. Ouyang, G. Sen, M. A. E. Anderson, "A New Method for Start-up of Isolated Boost Converters Using Magnetic-and Winding-Integration", *Applied Power Electronics Conference and Exposition (APEC)*, pp. 340-345, 2012

[29] T. Wu, Y. Chen, J. Yang, C. Kuo, "Isolated Bidirectional Full-Bridge DC-DC Converter with a Flyback Snubber", *Power Electronics, IEEE Transactions*, pp. 1915-1922, 2010

[30] S. Jalbrzykowski, T. Citko, "A bidirectional DC-DC converter for renewable energy systems", *Bulletin of the Polish Academy of Sciences*, Vol 57, 2009

[31] S. Jang, T. Lee, W. Lee, C. Won, "Bi-directional DC-DC Converter for Fuel Cell Generation System", *Power Electronics Specialists Conference*, pp. 4722-4728, 2004

[32] D. S. Segaran, "Dynamic Modeling and Control of Dual Active Bridge Bi-directional DC-DC Converter for Smart Grid Applications", Monash University

[33] R. Watson, F. C. Lee, "A Soft-Switched, Full-Bridge Boost Converter Employing an Active-Clamp Circuit", *Power Electronics Specialists Conference*, pp. 1948-1954, 1996

[34] A. Mousavi, P. Das, G. Moschopoulos, "A Comparative Study of New ZCS DC-DC Full-Bridge Boost Converter with a ZVS Active-Clamp Converter", *Power Electronics IEEE Transactions*, pp. 1347-1358, 2012

[35] O.A. Ahmed, J. Bleijs, "Optimized Active-Clamp Circuit Design for an Isolated Full-Bridge Current-Fed DC-DC Converter", *Power Electronics Systems and Applications (PESA)*, pp. 1-7, 2011

[36] Y. Miura, M. Kaga, Y. Horita, T. Ise, "Bidirectional Isolated Dual Full-bridge dc-dc Converter with Active Clamp for EDLC", *Energy Conversion Congress and Exposition (ECCE)*, pp. 1136-1143, 2010

[37] K. Wang, F. C. Lee, J. Lai, "Operation Principles of Bi-directional Full-bridge DC/DC Converter with Unified Soft-Switching Scheme and Soft-Starting Capability", *Applied Power Electronics Conference and Exposition*, pp. 111-118, 2000

[38] K. Wang, C.Y. Lin, L. Zhu, D. Qu, F.C. Lee, J.S. Lai, "Bi-directional DC to DC Converters for Fuel Cell Systems", *Power Electronics in Transportation*, pp. 47-51, 1998

[39] T. Kokilavani, G. Selvakumar, C. Christober Asir Rajan, "A ZVS Bidirectional dc-dc Converter Phase Shifted SPWM Control for Hybrid Electric and Fuel Cell Automotive Application", *Advances in Engineering, Science and Management*, pp. 700-703. 2012

[40] H. Xiao, S. Xie, "A ZVS Bidirectional DC-DC Converter with Phase-Shift Plus PWM Control Scheme", *Applied Power Electronics Conference, APEC 2007*, pp. 943 -948, 2007

[41] L. Zhu, K. Wang, F. C. Lee, J. S. Lai, "New Start-up Schemes for Isolated Full-Bridge Boost Converters", *Power Electronics IEEE Transactions*, pp. 946-951, 2003

[42] R. W. Erickson, D. Maksimovic, "Filter Inductor Design", *Fundamentals of Power Electronics*, Springer, 2001